EUROPEAN ORGANIZATION FOR NUCLEAR RESEARCH

CERN-PH-EP/2009-013
12 June 2009
Modified 20 September 2009

Σ^--antihyperon correlations in Z^0 decay and investigation of the baryon production mechanism

The OPAL Collaboration

Abstract

Data collected around $\sqrt{s}$ =91 GeV by the OPAL experiment at the LEP e^+e^- collider are used to study the mechanism of baryon formation. As the signature, the fraction of Σ^- hyperons whose baryon number is compensated by the production of a $\overline{\Sigma^-}$, $\overline{\Lambda}$ or $\overline{\Xi^-}$ antihyperon is determined. The method relies entirely on quantum number correlations of the baryons, and not rapidity correlations, making it more model independent than previous studies. Within the context of the JETSET implementation of the string hadronization model, the diquark baryon production model without the popcorn mechanism is strongly disfavored with a significance of 3.8 standard deviations including systematic uncertainties. It is shown that previous studies of the popcorn mechanism with $\Lambda\overline{\Lambda}$ and $p\pi\overline{p}$ correlations are not conclusive, if parameter uncertainties are considered.

(Submitted to Eur. Phys. J. C.)

The OPAL Collaboration

G. Abbiendi[2], C. Ainsley[5], P.F. Åkesson[7], G. Alexander[21], G. Anagnostou[1], K.J. Anderson[8], S. Asai[22], D. Axen[26], I. Bailey[25], E. Barberio[7,p], T. Barillari[31], R.J. Barlow[15], R.J. Batley[5], P. Bechtle[24], T. Behnke[24], K.W. Bell[19], P.J. Bell[1], G. Bella[21], A. Bellerive[6], G. Benelli[4], S. Bethke[31], O. Biebel[30], O. Boeriu[9], P. Bock[10], M. Boutemeur[30], S. Braibant[2], R.M. Brown[19], H.J. Burckhart[7], S. Campana[4], P. Capiluppi[2], R.K. Carnegie[6], A.A. Carter[12], J.R. Carter[5], C.Y. Chang[16], D.G. Charlton[1], C. Ciocca[2], A. Csilling[28], M. Cuffiani[2], S. Dado[20], M. Dallavalle[2], A. De Roeck[7], E.A. De Wolf[7,s], K. Desch[24], B. Dienes[29], J. Dubbert[30], E. Duchovni[23], G. Duckeck[30], I.P. Duerdoth[15], E. Etzion[21], F. Fabbri[2], P. Ferrari[7], F. Fiedler[30], I. Fleck[9], M. Ford[15], A. Frey[7], P. Gagnon[11], J.W. Gary[4], C. Geich-Gimbel[3], G. Giacomelli[2], P. Giacomelli[2], M. Giunta[4], J. Goldberg[20], E. Gross[23], J. Grunhaus[21], M. Gruwé[7], A. Gupta[8], C. Hajdu[28], M. Hamann[24], G.G. Hanson[4], A. Harel[20], M. Hauschild[7], C.M. Hawkes[1], R. Hawkings[7], G. Herten[9], R.D. Heuer[24], J.C. Hill[5], D. Horváth[28,c], P. Igo-Kemenes[a1], K. Ishii[22], H. Jeremie[17], P. Jovanovic[1], T.R. Junk[6,i], J. Kanzaki[22,u], D. Karlen[25], K. Kawagoe[22], T. Kawamoto[22], R.K. Keeler[25], R.G. Kellogg[16], B.W. Kennedy[19], S. Kluth[31], T. Kobayashi[22], M. Kobel[3,t], S. Komamiya[22], T. Krämer[24], A. Krasznahorkay Jr.[29,e], P. Krieger[6,l], J. von Krogh[10], T. Kuhl[24], M. Kupper[23], G.D. Lafferty[15], H. Landsman[20], D. Lanske[13], D. Lellouch[23], J. Letts[o], L. Levinson[23], J. Lillich[9], S.L. Lloyd[12], F.K. Loebinger[15], J. Lu[26,b], A. Ludwig[3,t], J. Ludwig[9], W. Mader[3,t], S. Marcellini[2], A.J. Martin[12], T. Mashimo[22], P. Mättig[m], J. McKenna[26], R.A. McPherson[25], F. Meijers[7], W. Menges[24], F.S. Merritt[8], H. Mes[6,a], N. Meyer[24], A. Michelini[2], S. Mihara[22], G. Mikenberg[23], D.J. Miller[14], W. Mohr[9], T. Mori[22], A. Mutter[9], K. Nagai[12], I. Nakamura[22,v], H. Nanjo[22], H.A. Neal[32], S.W. O'Neale[1,*], A. Oh[7], M.J. Oreglia[8], S. Orito[22,*], C. Pahl[31], G. Pásztor[4,g], J.R. Pater[15], J.E. Pilcher[8], J. Pinfold[27], D.E. Plane[7], O. Pooth[13], M. Przybycień[7,n], A. Quadt[31], K. Rabbertz[7,r], C. Rembser[7], P. Renkel[23], J.M. Roney[25], A.M. Rossi[2], Y. Rozen[20], K. Runge[9], K. Sachs[6], T. Saeki[22], E.K.G. Sarkisyan[7,j], A.D. Schaile[30], O. Schaile[30], P. Scharff-Hansen[7], J. Schieck[31], T. Schörner-Sadenius[7,z], M. Schröder[7], M. Schumacher[3], R. Seuster[13,f], T.G. Shears[7,h], B.C. Shen[4], P. Sherwood[14], A. Skuja[16], A.M. Smith[7], R. Sobie[25], S. Söldner-Rembold[15], F. Spano[8,x], A. Stahl[13], D. Strom[18], R. Ströhmer[30], S. Tarem[20], M. Tasevsky[7,d], R. Teuscher[8], M.A. Thomson[5], E. Torrence[18], D. Toya[22], I. Trigger[7,w], Z. Trócsányi[29,e], E. Tsur[21], M.F. Turner-Watson[1], I. Ueda[22], B. Ujvári[29,e], C.F. Vollmer[30], P. Vannerem[9], R. Vértesi[29,e], M. Verzocchi[16], H. Voss[7,q], J. Vossebeld[7,h], C.P. Ward[5], D.R. Ward[5], P.M. Watkins[1], A.T. Watson[1], N.K. Watson[1], P.S. Wells[7], T. Wengler[7], N. Wermes[3], D. Wetterling[10,b1], G.W. Wilson[15,k], J.A. Wilson[1], G. Wolf[23], T.R. Wyatt[15], S. Yamashita[22], D. Zer-Zion[4], L. Zivkovic[20]

[1]School of Physics and Astronomy, University of Birmingham, Birmingham B15 2TT, UK
[2]Dipartimento di Fisica dell' Università di Bologna and INFN, I-40126 Bologna, Italy
[3]Physikalisches Institut, Universität Bonn, D-53115 Bonn, Germany
[4]Department of Physics, University of California, Riverside CA 92521, USA
[5]Cavendish Laboratory, Cambridge CB3 0HE, UK
[6]Ottawa-Carleton Institute for Physics, Department of Physics, Carleton University, Ottawa, Ontario K1S 5B6, Canada

[7]CERN, European Organisation for Nuclear Research, CH-1211 Geneva 23, Switzerland
[8]Enrico Fermi Institute and Department of Physics, University of Chicago, Chicago IL 60637, USA
[9]Fakultät für Physik, Albert-Ludwigs-Universität Freiburg, D-79104 Freiburg, Germany
[10]Physikalisches Institut, Universität Heidelberg, D-69120 Heidelberg, Germany
[11]Indiana University, Department of Physics, Bloomington IN 47405, USA
[12]Queen Mary and Westfield College, University of London, London E1 4NS, UK
[13]Technische Hochschule Aachen, III Physikalisches Institut, Sommerfeldstrasse 26-28, D-52056 Aachen, Germany
[14]University College London, London WC1E 6BT, UK
[15]School of Physics and Astronomy, Schuster Laboratory, The University of Manchester M13 9PL, UK
[16]Department of Physics, University of Maryland, College Park, MD 20742, USA
[17]Laboratoire de Physique Nucléaire, Université de Montréal, Montréal, Québec H3C 3J7, Canada
[18]University of Oregon, Department of Physics, Eugene OR 97403, USA
[19]Rutherford Appleton Laboratory, Chilton, Didcot, Oxfordshire OX11 0QX, UK
[20]Department of Physics, Technion-Israel Institute of Technology, Haifa 32000, Israel
[21]Department of Physics and Astronomy, Tel Aviv University, Tel Aviv 69978, Israel
[22]International Centre for Elementary Particle Physics and Department of Physics, University of Tokyo, Tokyo 113-0033, and Kobe University, Kobe 657-8501, Japan
[23]Particle Physics Department, Weizmann Institute of Science, Rehovot 76100, Israel
[24]Universität Hamburg/DESY, Institut für Experimentalphysik, Notkestrasse 85, D-22607 Hamburg, Germany
[25]University of Victoria, Department of Physics, P O Box 3055, Victoria BC V8W 3P6, Canada
[26]University of British Columbia, Department of Physics, Vancouver BC V6T 1Z1, Canada
[27]University of Alberta, Department of Physics, Edmonton AB T6G 2J1, Canada
[28]Research Institute for Particle and Nuclear Physics, H-1525 Budapest, P O Box 49, Hungary
[29]Institute of Nuclear Research, H-4001 Debrecen, P O Box 51, Hungary
[30]Ludwig-Maximilians-Universität München, Sektion Physik, Am Coulombwall 1, D-85748 Garching, Germany
[31]Max-Planck-Institute für Physik, Föhringer Ring 6, D-80805 München, Germany
[32]Yale University, Department of Physics, New Haven, CT 06520, USA

[a] and at TRIUMF, Vancouver, Canada V6T 2A3
[b] now at University of Alberta
[c] and Institute of Nuclear Research, Debrecen, Hungary
[d] now at Institute of Physics, Academy of Sciences of the Czech Republic 18221 Prague, Czech Republic
[e] and Department of Experimental Physics, University of Debrecen, Hungary
[f] and MPI München
[g] and Research Institute for Particle and Nuclear Physics, Budapest, Hungary
[h] now at University of Liverpool, Dept of Physics, Liverpool L69 3BX, U.K.
[i] now at Dept. Physics, University of Illinois at Urbana-Champaign, U.S.A.

[j] now at University of Texas at Arlington, Department of Physics, Arlington TX, 76019, U.S.A.
[k] now at University of Kansas, Dept of Physics and Astronomy, Lawrence, KS 66045, U.S.A.
[l] now at University of Toronto, Dept of Physics, Toronto, Canada
[m] current address Bergische Universität, Wuppertal, Germany
[n] now at University of Mining and Metallurgy, Cracow, Poland
[o] now at University of California, San Diego, U.S.A.
[p] now at The University of Melbourne, Victoria, Australia
[q] now at IPHE Université de Lausanne, CH-1015 Lausanne, Switzerland
[r] now at IEKP Universität Karlsruhe, Germany
[s] now at University of Antwerpen, Physics Department,B-2610 Antwerpen, Belgium; supported by Interuniversity Attraction Poles Programme – Belgian Science Policy
[t] now at Technische Universität, Dresden, Germany
[u] and High Energy Accelerator Research Organisation (KEK), Tsukuba, Ibaraki, Japan
[v] now at University of Pennsylvania, Philadelphia, Pennsylvania, USA
[w] now at TRIUMF, Vancouver, Canada
[x] now at Columbia University
[y] now at CERN
[z] now at DESY
[a1] now at Gjøvik University College, Pb. 191, 2802 Gjøvik, Norway
[b1] now at MWM GmbH Mannheim, Germany
[*] Deceased

1 Introduction

The formation of baryons within a jet of hadrons has proved difficult to model and is still not well understood. While the shape of momentum spectra can be derived from QCD with the modified leading logarithmic approximation together with parton-hadron duality [1], more complex observables like correlations have not been derived from first principles.

Several physical models like the thermodynamic [2], cluster fragmentation [3] or string fragmentation [4, 5] models, have been developed to describe baryon production. Of these, the most successful is string fragmentation, based on the creation of diquark-antidiquark pairs from the vacuum as illustrated in figure 1. In a production chain of particles along the string, a baryon and an antibaryon can be produced in immediate succession (figs. 1a,b) or else one or more intermediate mesons can be produced between them (figs. 1c-e). This production of intermediate mesons, referred to as the popcorn effect [6, 7], is included as an option in the Monte Carlo event generators JETSET and PYTHIA [8, 9] and can be steered with a free parameter.

Past experimental investigations of the popcorn effect made use of rapidity ordering of hadrons in the fragmentation chain. Intermediate mesons modify the rapidity difference between associated baryons and antibaryons. Rapidity correlations between $\Lambda\,\overline{\Lambda}$ pairs produced in Z^0 decays have been studied by several LEP collaborations and the conclusion was that best agreement between the experiments and the JETSET Monte Carlo model [8] was obtained

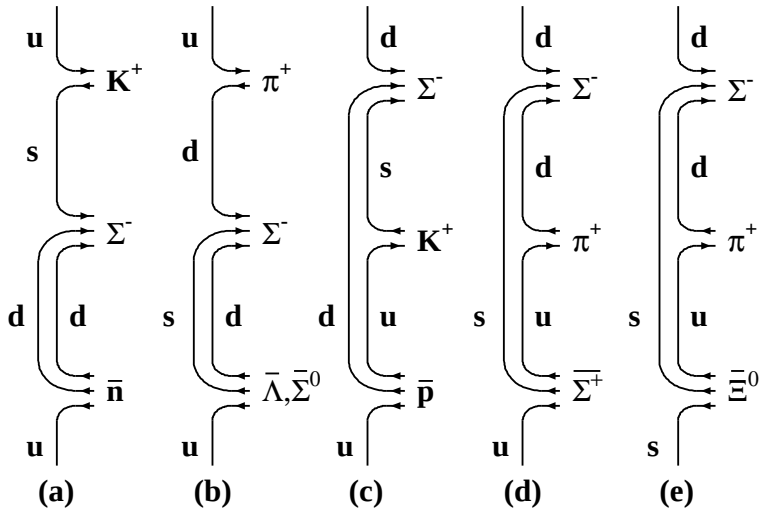

Figure 1: *Baryon production in the diquark model without (a,b) and with (c-e) the popcorn effect.*

with the popcorn effect included [10]-[12].

A contradictory result was reported by the DELPHI collaboration [13]. Their measurement is based on triple correlations between a proton, an antiproton and a charged pion close in rapidity. Because the popcorn effect enhances the pion density in the rapidity interval between the proton and antiproton, the minimum rapidity difference between a pion and a proton was compared for the particle orderings $p\pi\overline{p}$ and $\pi p\overline{p}$. The measurement indicated that the rapidity rank correlations could be reproduced without the popcorn effect. The contribution of events with popcorn produced mesons was reported to be less than 15% at 90% confidence level. Insufficient modeling of the fragmentation dynamics could not, however, be excluded [13].

In this analysis, the popcorn mechanism is investigated in a different way, by tagging rare baryons and measuring the quantum numbers of correlated antibaryons. By not relying on rapidity differences, we obtain results that are more model-independent than previous studies. The data were collected with the OPAL experiment at the LEP e^+e^- collider at CERN. Especially suitable for our purposes is the Σ^- hyperon. If a Σ^- is produced, its baryon number and strangeness are compensated either by an antinucleon and a kaon, as

illustrated in figure 1a, or by an associated antihyperon. The case of $\overline{\Lambda}$ or $\overline{\Sigma^0}$ production without the popcorn effect is shown in figure 1b. The same graph, with the bottom-most u-quark replaced by a d- or s-quark, describes associated $\overline{\Sigma^-}$ and $\overline{\Xi^-}$ production. Associated production of a $\overline{\Sigma^+}$ and $\overline{\Xi^0}$ antihyperon with a Σ^- can only occur through the popcorn mechanism (figs. 1d,e). This makes $\Sigma^-\overline{\Sigma^+}$ and $\Sigma^-\overline{\Xi^0}$ correlations ideal tools to study the popcorn effect. Unfortunately, the production rate of Σ^- hyperons and the probabilities for simultaneous reconstruction of Σ^- and $\overline{\Sigma^+}$ or Σ^- and $\overline{\Xi^0}$ particles are too small to make such an analysis feasible, given the available data statistics. The equivalent analysis cannot be performed with tagged Λ hyperons because in this case $\overline{\Sigma^+}$ and $\overline{\Xi^0}$ antihyperons can be produced without the popcorn effect. Alternatively one can measure the fraction

$$F_{\overline{H}} = F_{\Sigma^-,\overline{\Sigma^-}} + F_{\Sigma^-,\overline{\Lambda}} + F_{\Sigma^-,\overline{\Xi^-}} \tag{1}$$

of Σ^- hyperons accompanied by a $\overline{\Sigma^-}$ ($F_{\Sigma^-,\overline{\Sigma^-}}$), a $\overline{\Lambda}$ ($F_{\Sigma^-,\overline{\Lambda}}$) or a $\overline{\Xi^-}$ ($F_{\Sigma^-,\overline{\Xi^-}}$). These correlations can occur in the popcorn model but are more likely in the diquark model (fig. 1b) and their rate is thus a sensitive measure of the baryon production mechanism.

The exact definition of the three correlations $F_{\Sigma^-,\overline{k}}$ in the sum (1) needs to account for the possibility that an event may contain more than one Σ^- hyperon, other additional hyperons, or more than one antihyperon. More generally, one can consider an arbitrary particle k and its antiparticle $\overline{k}$. If the number of Σ^- hyperons in an event is larger than 1, all combinations of Σ^- $\overline{k}$ and Σ^- k pairs are counted. Denoting the total rates of Σ^--antiparticle and Σ^--particle pairs by $R_{\Sigma^-,\overline{k}}$ and $R_{\Sigma^-,k}$, respectively, and the total Σ^- rate by R_{Σ^-}, the fraction $F_{\Sigma^-,\overline{k}}$ can be written as

$$F_{\Sigma^-,\overline{k}} = \frac{R_{\Sigma^-,\overline{k}} - R_{\Sigma^-,k}}{R_{\Sigma^-}} \ . \tag{2}$$

This definition implies that the $n_{\overline{k}}$ antiparticles $\overline{k}$ in an event enter $n_{\overline{k}}\, n_{\Sigma^-}$ times. The Σ^- Σ^- pairs are counted $n_{\Sigma^-}\,(n_{\Sigma^-}-1)$ times. In the data analysis, this multiple counting is not an issue because the number of reconstructed Σ^- hyperons per event is very small. Baryon number conservation ensures that $\sum_{\overline{k}} F_{\Sigma^-,\overline{k}} = 1$, if the sum extends over all antibaryons, including the antihyperons and antinucleons. It is the understanding throughout this paper that the charge conjugated channels are included. Thus, the rates $R_{\Sigma^-,k}$ contain all like-sign pairs Σ^- k and $\overline{\Sigma^-}$ $\overline{k}$, the rates $R_{\Sigma^-,\overline{k}}$ contain all unlike-sign pairs Σ^- $\overline{k}$ and $\overline{\Sigma^-}$ k, and $\overline{\Sigma^-}$ antihyperons are included in R_{Σ^-}.

It is evident from figure 1c that kaons created through the popcorn effect reduce $F_{\overline{H}}$. The PYTHIA Monte Carlo program without the popcorn effect, tuned to reproduce the observed baryon rates and momentum spectra, predicts $F_{\overline{H}} \approx 0.9$, as will be shown later. The other extreme is a model in which baryon number and strangeness are compensated statistically, i.e. from conservation laws alone. The ratio of weakly decaying hyperon to total baryon production in Z^0 decays is approximately 0.22 [14]. Because there must be at least one antibaryon in the rest of the event, if the Σ^- is detected, and the tagging biases the number of strange valence antiquarks, the lower bound will be a bit larger: $F_{\overline{H}} > 0.22$. A more rigorous calculation can be performed with the thermodynamic model for particle production. The advanced version of the model, based on the microcanonical ensemble, yields $F_{\overline{H}} = 0.23$ for an initial system without strangeness [15], close to the simple estimate of the lower bound.

2 Event selection

2.1 Event topologies

In any experiment with a sufficiently large tracking device Σ^- hyperons can be identified by track kinks from $\Sigma^- \to \mathrm{n}\pi^-$ decays. At LEP energies, the efficiency is much less than 100%, because the decay vertex lies often outside the fiducial volume for its reconstruction. In principle, correlated decays $\overline{\Sigma^-} \to \overline{\mathrm{n}}\pi^+$ and $\overline{\Xi^-} \to \overline{\Lambda}\pi^+$ could be reconstructed using track kinks, too, but the efficiency for the exclusive reconstruction of $\Sigma^-\ \overline{\Sigma^-}$ or $\Sigma^-\ \overline{\Xi^-}$ pairs is small.

In this work, only the Σ^- hyperons were reconstructed exclusively. Two signatures for correlated antihyperons were used:

1. $\overline{\Lambda}$ hyperons were reconstructed by analyzing their so-called V^0 topology from the decay $\overline{\Lambda} \to \overline{\mathrm{p}}\pi^+$. The decay vertex and the flight direction of the $\overline{\Lambda}$ candidates allow the $\overline{\Lambda}$ impact parameters d_0 with respect to the beam line to be computed. Direct $\overline{\Lambda}$ production, including the contribution of decays from $\overline{\Sigma^0}$ hyperons, is characterized by low impact parameters d_0, while large impact parameters indicate a preceding weak decay and are a signature for $\overline{\Xi}$ decays.

2. Charged pions with significant impact parameters are a signature for weak decays of arbitrary antihyperons. An inclusive sample of tracks with large d_0 values, consistent with a pion interpretation, was selected. Throughout this paper, this data set is referred to as the sample of displaced tracks. This sample has a large background, and different antihyperon species contribute with different weights, because the number of decay pions per antihyperon is 1 for $\overline{\Sigma^-}$, 0.64 for $\overline{\Lambda}$ and 1.64 for chain decays of $\overline{\Xi^-}$.

The correlated $\Sigma^-\overline{\Lambda}$ candidate sample gives the numbers of true $\Sigma^-\ \overline{\Lambda}$ and $\Sigma^-\ \overline{\Xi^-}$ pairs. The fraction $F_{\overline{\Sigma^-}}$ can be extracted from the displaced track sample by a weighted subtraction of the $\Sigma^-\ \overline{\Lambda}$ and $\Sigma^-\ \overline{\Xi^-}$ contributions.

2.2 Experiment and data sets

All data taken by the OPAL experiment [16] in the Z^0 energy region during the years 1991 to 2000 were analyzed to measure the correlation. The OPAL experiment had nearly complete solid angle coverage and excellent hermeticity. The innermost part of the central tracking detector was a high-resolution silicon microvertex detector, which immediately surrounded the beam-pipe [17]. It was followed by a high-precision vertex drift chamber, a large-volume jet chamber [18], and z-chambers, all in a uniform 0.435 T axial magnetic field. In this work, the outer detector parts as well as the forward detector system were needed for triggering and identification of multihadronic events only. The criteria for multihadronic event selection have been described elsewhere [19].

The present analysis is entirely based on the central tracking system [16, 18]. For candidates to be accepted, all central wire chambers and the microvertex detector were required to be fully operational. The data sample for this analysis consists of 3.97 million events.

The identification of strange particles is based on earlier work [20, 21]. The innermost sense wires of the jet chamber had a distance of 25.5 cm from the beam spot, the wire-to-wire distance was 1 cm and there were 159 sensitive radial layers. The requirement of the pattern recognition program was the existence of at least 12 hits in the jet chamber. This makes it possible to identify Σ^- hyperons with decay lengths larger than 36 cm.

The z coordinate, along an axis parallel to the electron beam, was measured with a precision of 700 μm with the stereo wires of the vertex chamber and 100 to 350 μm with the z chambers. For tracks leaving the drift chamber at the side cones, the z coordinates of the exit points can be computed from the radius of the last wire with a hit. At the beam spot a constraint can be set using the bunch length of the beam. Inside the jet chamber, the z coordinates were measured with the charge division method with a resolution of 6 cm. This is one limiting factor for the kinematical reconstruction of Σ^- hyperons to be discussed later.

The quality of the impact parameter measurement is directly connected to the detector resolutions in the (r, φ) plane perpendicular to the beam axis. These resolutions were 5 μm to 10 μm for the microvertex detector [17], 55 μm for the vertex chamber and, on average, 135 μm for the jet chamber [16].

To study the detector response, the selection was applied also to Monte Carlo samples used before at OPAL. These were generated with the JETSET7.3 and JETSET 7.4 programs, followed by a full detector simulation [22]. The steering parameters for the generator are given in [23, 24]. The subset of parameters relevant for this analysis is discussed in section 4.2 and the numerical values are given in table 8 (appendix). In total, the Monte Carlo samples consisted of 4.65 million multihadronic Z^0 decays.

2.3 Σ^- Selection

The production cross section of Σ^- hyperons has previously been measured by OPAL [20]. Here the selection criteria to find track pairs forming a decay vertex were slightly changed relative to [20] to improve the sensitivity of the analysis to correlations. The applied cuts are summarized in table 1. They accommodate pattern recognition tolerances and define a fiducial jet chamber volume to guarantee minimal hit numbers for both tracks and to remove background from the end plates. The ratio l_1/p_1 in the last line of table 1 is proportional to the decay time in the rest frame of the decaying particle. High values are rejected to reduce the substantial background from kaon decays.

variable	condition
transverse momenta of the decaying and the daughter particle	$p_{T1} > 0.15$ GeV/c, $p_{T2} > 0.10$ GeV/c
total momentum of the decaying particle	$p_1 > 2$ GeV/c
impact parameter of the primary track	$d_0 < 5$ cm
endpoint radius of the primary track	$r_{E1} < 170$ cm
maximum gap between the primary and the secondary track in the (r, φ) plane	$d_{12} < 10$ cm
number of secondary tracks	1
particle charges	equal
arc distance between the intersection point and the end points of tracks 1,2 in (r, φ)	$\mu_1 > -7$ cm, $\mu_2 < +7$ cm
radius of the intersection point	$r_{Vtx} > 35$ cm
distance of the intersection point from the end plate in z direction	$\Delta z_{Vtx} > 40$ cm
χ^2 for agreement of the two tracks in the (r, φ) plane, using (3×3) error matrix	$\chi^2 > 2000$
ratio of the track length to the momentum of the decaying particle	$l_1/p_1 < 15$ cm/(GeV/c)

Table 1: *Selection of track pairs forming a decay vertex (for a more detailed description of the variables, see [20]).*

Monte Carlo studies show that the following processes have to be considered as sources for Σ^- candidates, others being negligible [20]:

1. $\Sigma^- \to \mathrm{n}\pi^-$;
2. $\overline{\Sigma^+} \to \overline{\mathrm{n}}\pi^-$;
3. $\Xi^- \to \Lambda\pi^-$;
4. $\mathrm{K}^- \to \pi^-$+neutrals; $\mathrm{K}^- \to \mu^-$+neutrals or $\mathrm{K}^- \to e^-$+neutrals;
5. secondary reactions in the detector material and fake background. The last sample consists mainly of scattered particles.

To determine the relative contributions of these processes to the observed data sample, an unfolding procedure very similar to that used in [20] was used. The invariant mass m_{Σ^-} and the decay angle θ^* of the pion candidate in the rest frame of the hypothetical Σ^- particle were computed, assuming that the unseen neutral particle is a neutron. The angle θ^* is defined with respect to the flight direction of the Σ^- candidate at the decay vertex.

Figure 2 shows scatter plots of these variables for the data and three Monte Carlo sources of events with kinked tracks, namely events with Σ^-, Ξ^- or K^- in the final state. The background 5, not shown in figure 2, is a smooth function of both observables and is largest in the backward direction $\cos\theta^* = -1$.

Five two-dimensional regions, denoted by $a, ...e$, were introduced in the $(m_{\Sigma^-}, \cos\theta^*)$ plane to enrich dedicated kink sources (see figure 2). The bin number of a Σ^- candidate was used as an observable in the unfolding procedure to be described in section 3.

In total, 16790 candidates were found in the two-dimensional plane in the mass range from threshold to 1.5 GeV. In the Monte Carlo sample 18754 kinks were identified.

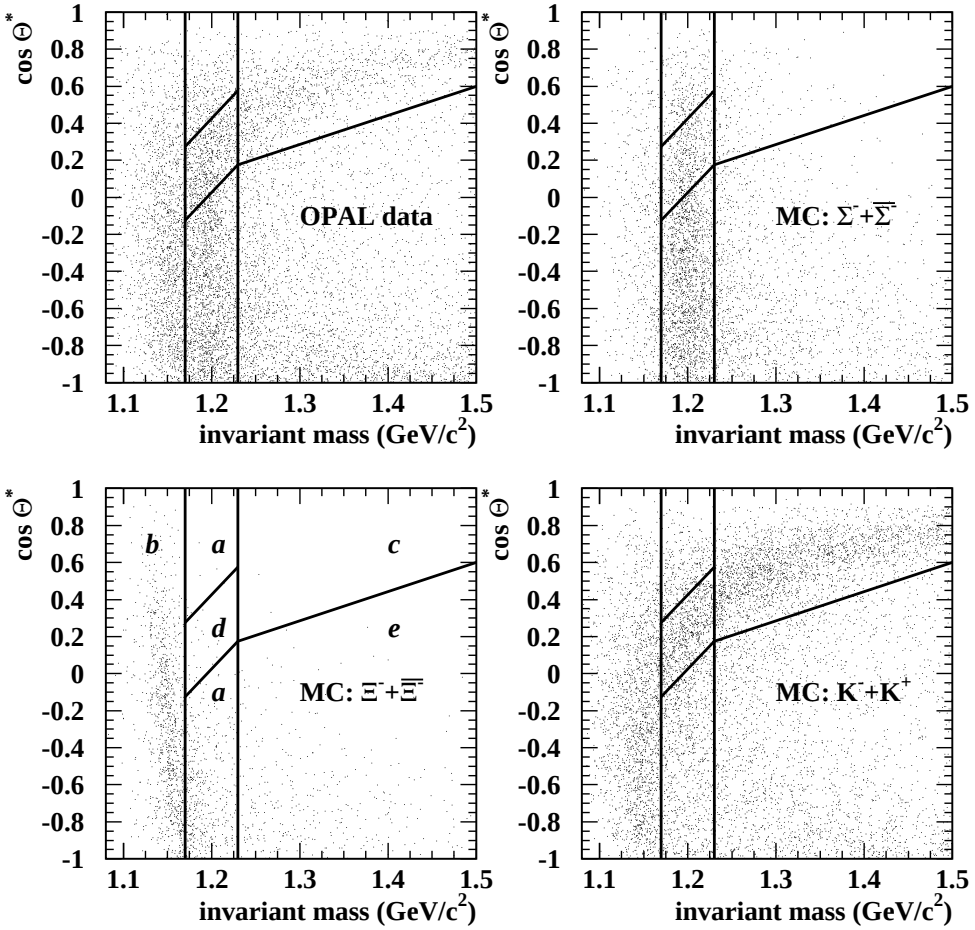

Figure 2: *Definition of two-dimensional bins to disentangle Σ^- hyperons from background. The reconstructed mass is plotted versus the pion emission angle in the hypothetical center-of-mass system. Top left: data. Other plots: Monte Carlo simulations for three particle classes as indicated. The labeling of the two-dimensional bins is shown in the bottom left plot. The preferential bins for the kink sources are: a+d for Σ^- and $\overline{\Sigma^+}$, b for Ξ^-, b,c and d for K^- and e for background.*

2.4 Selection of pions from weak decays

Two pre-cuts were applied to select tracks with a good reconstruction quality: the transverse momentum with respect to the beam had to be larger than 0.15 GeV/c and the track angle at the beam spot relative to the beam direction was restricted to the region $|\cos\theta| \leq 0.80$.

To remove charged particles from charm or bottom decays, the impact parameter $d_{0,\pi}$ with respect to the primary vertex was required to be larger than 0.2 cm. This cut is the essential condition to define the sample of displaced tracks. A lower value would be sufficient but does not improve the accuracy of the correlation analysis.

Pions were enriched using the specific energy loss measurement of the central drift chamber [26]. A weight $w_{dE/dx}(\pi)$ was defined as the probability that the energy loss dE/dx of a pion deviates from the median value $< dE/dx > (\pi)$ by more than the measured difference from the median value. The applied condition was $w_{dE/dx}(\pi) > 0.02$ and the number of hits contributing to this measurement had to be at least 20.

Finally, the angle between the momenta of the pion candidate and the Σ^- candidate at the primary vertex was required to be less than 90 degrees. This hemisphere cut is motivated by the fact that it rarely happens that baryon number and strangeness are compensated by an antihyperon in the opposite event hemisphere. The cut reduces the combinatorial background by a factor 2.

In total, 9965 correlated like-sign $\Sigma^-\pi^-$ and 11951 unlike-sign $\Sigma^-\ \pi^+$ pair candidates were selected with these cuts. The corresponding results for the Monte Carlo sample are 10769 and 13818, respectively. If the total number of Monte Carlo track kinks is scaled to the observation, the number of like-sign pairs in the data is well reproduced by the Monte Carlo, the difference being $(+3.4 \pm 1.4)\%$. The observed unlike-sign minus like-sign difference, however, deviates from the prediction by $(-28 \pm 7)\%$. This deficit, already visible at raw data level, indicates that the Monte Carlo sample contains too many correlated antihyperons and is the basis for the final result of this paper.

2.5 Λ Selection

The selection cuts to find Λ decays in the central drift chamber have been described in [21]. The preselection cuts were relaxed from those of [21]. In this analysis all candidates with reconstructed masses between the pπ threshold and 1.20 GeV/c^2 were accepted. This larger mass window was needed to study the non-Λ background.

Two criteria were added. If the reconstructed Λ flight path points back to the (r, φ) position of the hypothetical Σ decay kink within 2 degrees, it was assumed that the kink originated from a $\Xi^- \rightarrow \Lambda\pi^-$ decay and the Λ candidate was dropped. The cut removed approximately 3/4 of the like sign $\Xi^-\ \Lambda$ ($\overline{\Xi^-}\ \overline{\Lambda}$)-pairs and reduced the self-correlation of Ξ^- particles with their own decay Λ's accordingly.

Secondly, the hemisphere cut applied to the decay pions was also applied to the Λ's. The

angle between the flight directions of Σ and $\overline{\Lambda}$ at the primary vertex was required to be less than 90 degrees.

For the correlation analysis, the mass window was reduced to a ± 10 MeV wide interval around the true Λ mass. Totals of 276 $\Sigma^-\Lambda$ ($\overline{\Sigma^-}\,\overline{\Lambda}$) and 604 $\Sigma^-\,\overline{\Lambda}$ ($\overline{\Sigma^-}\,\Lambda$) pair candidates passed all selection cuts. In the Monte Carlo sample 284 like-sign and 721 unlike-sign pairs were found. The observed unlike-sign minus like-sign difference is smaller than the Monte Carlo prediction by $(16 \pm 11)\%$, if normalized to the number of observed kinks.

3 Correlation analysis

3.1 Unfolding of kink sources

From the Monte Carlo sample one gets, for every kink source i and every two-dimensional $(m_{\Sigma^-}, \cos\theta^*)$ bin j, the number of accepted events $K_i^{(MC)}(j)$. The populations of the bins $j = a,\ldots e$ in figure 2 are sensitive to the invariant mass and θ^* resolutions, which in turn depend on the z resolution of the central drift chamber. The z coordinate, however, is not well modeled in the Monte Carlo simulation. Because the track end points in the jet chamber are well known by other measurements, this mismodeling at the decay vertex gives the dominant contribution to the systematic error of the Σ^- rate [20]. To correct the Monte Carlo program for it, the z components of all Σ momenta were modified according to $p_{z\cdot new} = p_{z,rec} + c\cdot(p_{z,rec} - p_{z,true})$, where $p_{z,true}$ is the true momentum from the MC generator and $p_{z,rec}$ the reconstructed momentum. The constant c is one common factor to be determined in the analysis.

The total number of kinks $K(j)$ expected in bin j is given by

$$K(j) = \sum_i \xi_i \frac{N_{data}}{N_{MC}} \cdot K_i^{(MC)}(j) \ , \tag{3}$$

where N_{data} and N_{MC} are the total number of multihadronic data and Monte Carlo events, respectively. Incorrect Monte Carlo rates are corrected for by the five scaling factors ξ_i. If they are known, the true production rates per multihadronic event, R_i, can be computed for all sources i, for example

$$R_{\Sigma^-} = \xi_{\Sigma^-} \cdot R_{\Sigma^-}^{(MC)} \quad \text{with} \quad R_{\Sigma^-}^{(MC)} = \sum_j K_{\Sigma^-}^{(MC)}(j) \ . \tag{4}$$

Contrary to [20] the factors ξ_i were treated as momentum independent, because the analysis of [20] had shown that the modeling of the spectral shape was satisfactory. The contribution from $\overline{\Sigma^+}$ hyperons to $K(j)$ is less than 20% of that of the Σ^- particles [20]. The ratio of the genuine production rates, approximately 1 due to isospin symmetry, was fixed to the Monte Carlo prediction, so that $\xi_{\overline{\Sigma^+}} = \xi_{\Sigma^-}$. Four scaling factors ξ_i were thus left for adjustment. They were computed with a χ^2-fit of the measured kink rates to equation (3) for a given value of c.

It was then checked whether the Monte Carlo simulation reproduces the reconstructed mass and $\cos\theta^*$ distributions. Differing from our previous analysis [20], the proportionality factor c was chosen to get the lowest χ^2-sum for both distributions. The best overall agreement was found for $c = 1.35$ with a one-sigma interval ranging from 1.32 to 1.45. The final fit result is shown in figs. 3 and 4. The agreement is excellent. The error of c is not included in the statistical errors of the ξ_i. It is treated separately as a contribution to the systematic error.

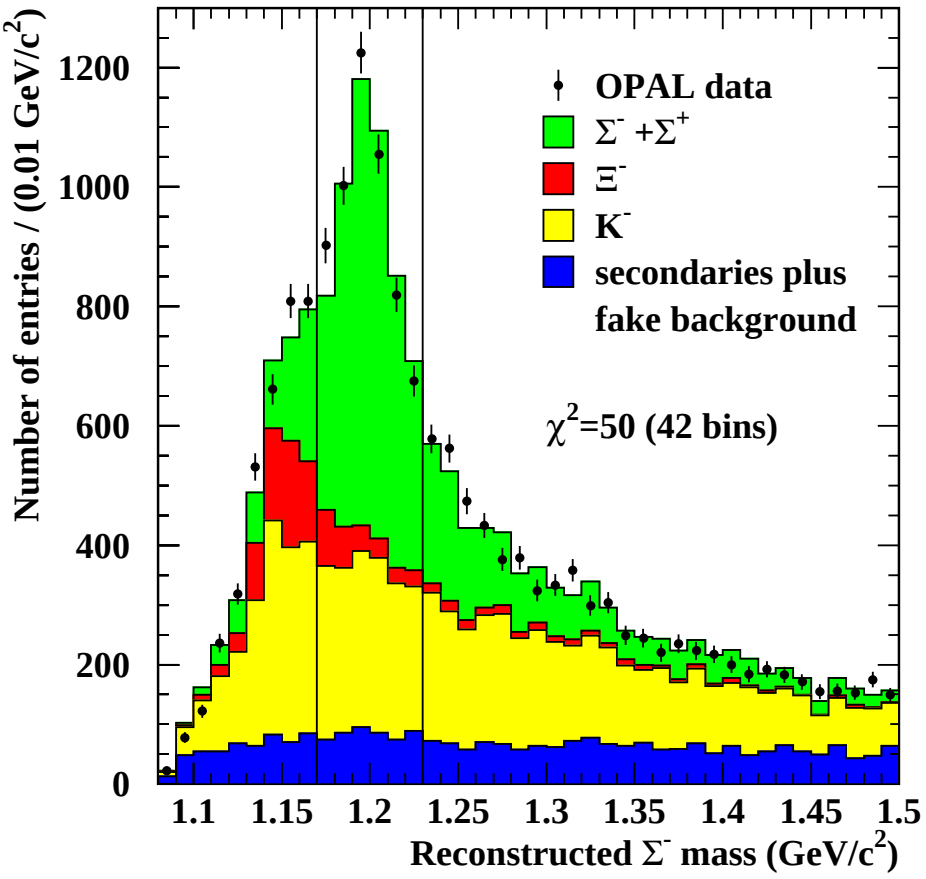

Figure 3: *Measured Σ^- mass spectrum. Points: data. Histograms: results of the fit, ordered according to the sources for track kinks. The plotted errors are the statistical errors of the data.*

The $\Sigma^- + \overline{\Sigma^-}$ production rate was found to be $R_{\Sigma^-} = 0.073 \pm 0.004$. According to [20] a systematic error of ± 0.009 has to be added. Within the total error, this result is consistent with our published value $R_{\Sigma^-} = 0.083 \pm 0.011$ and also with the world average $R_{\Sigma^-} = 0.082 \pm 0.007$ [14]. The difference is mainly due to the modified treatment of the z-resolution.

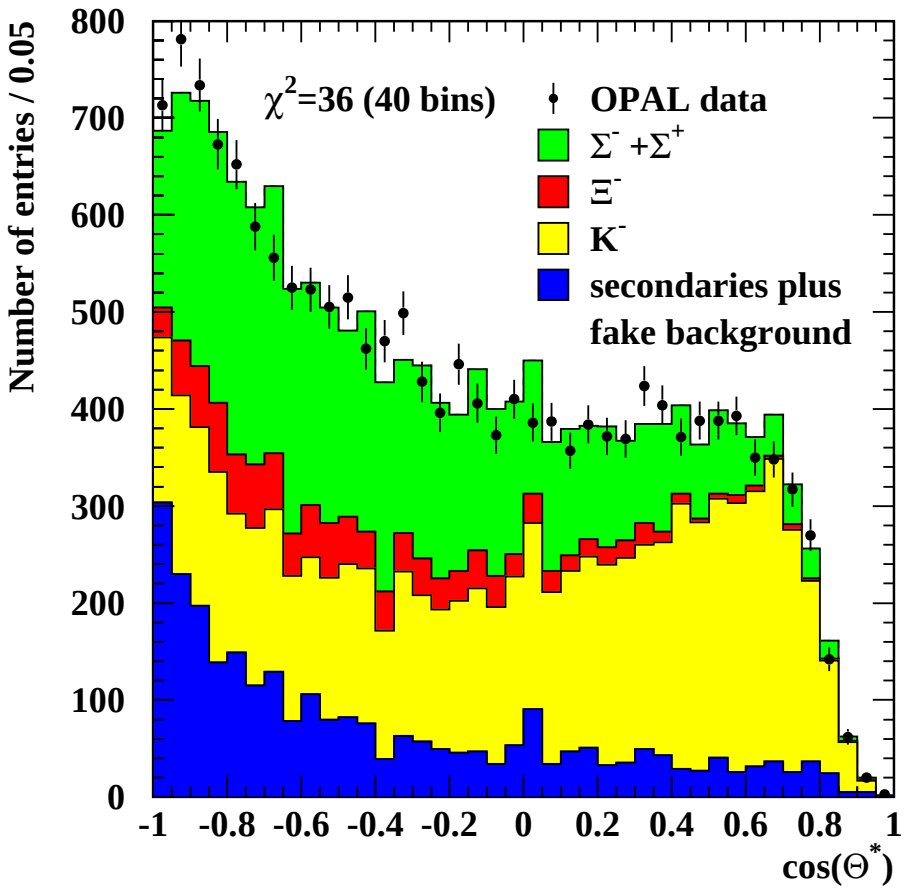

Figure 4: *Cosine of the center-of-mass pion emission angle. Points: data. Histograms: results of the fit, ordered according to the sources for track kinks. The plotted errors are the statistical errors of the data.*

3.2 Correlated particle sources

The correlated rates of kink-V^0 or kink-displaced-track pairs were measured as a function of the bin number j and the impact parameter d_0 of the correlated particle relative to the beam line. The variable d_0 contains information on the lifetime of the parent particle of the correlated particle in case of a preceding weak decay, and is needed to disentangle correlated $\overline{\Lambda}$'s from $\overline{\Xi}$'s decaying into $\overline{\Lambda}$'s.

In the Monte Carlo simulation, nine sources have to be considered for the displaced tracks and correlated V^0's:

1. $\overline{\Sigma^-} \rightarrow \overline{\mathrm{n}}\pi^+$;
2. $\overline{\Sigma^+} \rightarrow \overline{\mathrm{n}}\pi^-$ or $\overline{\mathrm{p}}\pi^0$;
3. $\overline{\Xi^-} \rightarrow \overline{\Lambda}\pi^+ \rightarrow \overline{\mathrm{p}}\pi^+\pi^+$;
4. $\overline{\Xi^0} \rightarrow \overline{\Lambda}\pi^0 \rightarrow \overline{\mathrm{p}}\pi^+\pi^0$;
5. $\overline{\Lambda} \rightarrow \overline{\mathrm{p}}\pi^+$, including $\overline{\Lambda}$ antihyperons from $\overline{\Sigma^0}$ decays, but without the contributions from $\overline{\Xi}$ decays;
6. charged particles from K^+ decays;
7. charged particles or V^0 configurations from K^0 decays;
8. non-K^0 background of the V^0 topology;
9. displaced tracks from secondary interactions, mainly scattering.

All sources, except for the eighth one, contribute to the sample of displaced tracks. For V^0-like events only the sources 3,4,5,7 and 8 are relevant. The sample of displaced tracks is enriched in pions but contains also a small fraction of protons and leptons. These contaminations are included in the Monte Carlo rates and are classified according to the above scheme.

The combination of five kink sources with nine correlated particle sources leads to a total number of 45 classes of particle pairs. In addition, one has to distinguish between like-sign and unlike-sign pairs. Equation (3) can be generalized to the like-sign pair rate $D^{like}(j, d_0)$ and the difference of the unlike-sign pair rate $D^{unlike}(j, d_0)$ and $D^{like}(j, d_0)$,

$$D^{like}(j, d_0) = \sum_{i,k} \eta^{(l)}_{i,k} \cdot \frac{N_{data}}{N_{MC}} \cdot D^{(MC,like)}_{i,k}(j, d_0) \ ; \tag{5}$$

$$D^{unlike}(j, d_0) - D^{like}(j, d_0) = \sum_{i,k} \eta^{(a)}_{i,k} \cdot \frac{N_{data}}{N_{MC}} \cdot (D^{(MC,unlike)}_{i,k}(j, d_0) - D^{(MC,like)}_{i,k}(j, d_0)) \ . \tag{6}$$

The indices at the Monte Carlo rates $D^{(MC,like)}_{i,k}$ and $D^{(MC,unlike)}_{i,k}$ specify the kink source i and the correlated particle source k, respectively. The parameters $\eta^{(l)}_{i,k}$ and $\eta^{(a)}_{i,k}$ are 90 scaling

kink source	correlated particle					
	$\overline{\Sigma^-}$	$\overline{\Sigma^+}$	$\overline{\Xi^-}$	$\overline{\Xi^0}$	$\overline{\Lambda}$	K^+
Σ^-	0.33	0.014	0.15	0.01	0.28	0.04
Σ^+	0.01	0.32	0.01	0.14	0.28	0.024
Ξ^-	0.34	0.026	0.15	0.029	0.36	0.45
K^-	< 0.01	< 0.01	< 0.01	< 0.01	0.03	0.50

Table 2: *Fractions $F_{i,k}^{(MC)}$ as predicted by the PYTHIA 6.1 generator with the parameters from ref [24].*

factors. In principle, they have to be extracted with a combined fit of the j and d_0 dependent distributions of kink-track pairs and kink-V^0 pairs to equations (5) and (6).

The Monte Carlo generator predicts the generic correlations $F_{i,\overline{k}}^{(MC)}$, defined with equation (2), generalized to arbitrary sources i and k. Table 2 gives the results for hyperon-antiparticle correlations at generator level for the most recent parameter set used by the OPAL experiment [24].

If the scaling factors $\eta_{i,k}^{(a)}$ are known, the experimental results for the correlations can be computed

$$F_{i,\overline{k}} = \frac{\eta_{i,k}^{(a)}}{\xi_i} \cdot F_{i,\overline{k}}^{(MC)} \ . \tag{7}$$

Here, the scaling factors ξ_i from the kink fit (section 3.1) enter.

The factors $\eta_{i,k}^{(l)}$ are only needed to parameterize the statistical errors for the fit using equation (6). With very few exceptions, they are close to one and no physical result is extracted from them.

3.3 Evaluation of the correlation matrix

In spite of the large number of scaling factors $\eta_{i,k}^{(a)}$, a reliable fit of the data can be obtained. This can be seen from the integrals of the differences $(D_{i,k}^{(MC,unlike)}(j,d_0) - D_{i,k}^{(MC,like)}(j,d_0))$ over the variables $m_{\Sigma^-}, \cos\theta^*$ and d_0, listed in tables 3 and 4. The entries in the tables are normalized to the total differences, using $\eta_{i,k}^{(a)} = 1$, and thus show the relative importance of the terms. The nine most significant correlations are given in the tables, the individual contributions of all other sources being less than 2%. In total, the entries in table 3 for displaced tracks account for 96% of the total rate difference. The contributions to the V^0 in table 4 add up to 104%, the excess being compensated by a small amount of $\Sigma^+\overline{\Lambda}$ correlations with the opposite sign.

The scaling factors for the four largest correlations in tables 3 and 4, $\eta_{\Sigma^-,\overline{\Sigma^-}}^{(a)}$, $\eta_{\Sigma^-,\overline{\Lambda}}^{(a)}$, $\eta_{\Sigma^-,\overline{\Xi^-}}^{(a)}$ and $\eta_{\Xi^-,\overline{\Lambda}}^{(a)}$, are determined with the fit. Three of them are needed to compute $F_{\overline{H}}$.

kink source	displaced track source				
	$\overline{\Sigma^-}$	$\overline{\overline{\Xi^-}}$	$\overline{\Lambda}$	K^+	background
Σ^-	$(27 \pm 1)\%$	$(16 \pm 1)\%$	$(10 \pm 1)\%$		$(17 \pm 4)\%$
Ξ^-	$(12 \pm 1)\%$	$(6 \pm 1)\%$	$(5 \pm 1)\%$		
K^-				$(3 \pm 1)\%$	
kink background					

Table 3: *Largest contributions to the correlations between kinks and displaced tracks.*

kink source	V^0 source		
	$\overline{\overline{\Xi^-}}$	$\overline{\Lambda}$	V^0 background
Σ^-	$(20 \pm 2)\%$	$(43 \pm 3)\%$	$(14 \pm 3.5)\%$
Ξ^-	$(6 \pm 1.5)\%$	$(21 \pm 2)\%$	

Table 4: *Largest contributions to the correlations between kinks and V^0 candidates.*

The data statistics do not allow to fit more than four parameters. The remaining η's were thus fixed by symmetry considerations, isospin invariance or Monte Carlo studies. Systematic errors were assigned to them, if necessary. In the following, a few examples are described, preferentially the correlations in tables 3,4.

For symmetry reasons, one has

$$\eta^{(a)}_{\Xi^-,\overline{\Sigma^-}} = \eta^{(a)}_{\Sigma^-,\overline{\Xi^-}} \ . \tag{8}$$

There is no model independent prediction for $F_{\Xi^-,\overline{\Xi^-}}$. This parameter was set to the original Monte Carlo result. It follows then from equation (7) that

$$\eta^{(a)}_{\Xi^-,\overline{\Xi^-}} = \xi_{\Xi^-} \ . \tag{9}$$

It has been checked for various acceptable Monte Carlo generator tunings, described in the next section, that this procedure is valid within 20%.

Non-negligible parts of the correlation are introduced by the correlated particle backgrounds 8 and 9; they are given as sums over the kink sources in tables 3 and 4. The origin of this effect is charge conservation in the events. Since the displaced-track-background consists mainly of scattered particles, it reflects the original particle charges. The kink selection introduces a charge bias for the rest of the event, which is visible in the ensemble of remaining charged particles on a statistical basis. This is true not only for scattered particles, but also for asymmetric fake V^0 candidates. Kinks and correlated particles are assigned to each other by chance. The condition $\eta^{(a)}_{i,track} = \eta^{(a)}_{i,V^0} = \xi_i$ was introduced, assuming a correct modeling of the background sources 8 and 9. This is justified because the equivalent relation for the like-sign background rates was confirmed with a fit to the data with the parameterizations $\eta^{(l)}_{i,track} = \xi_i \zeta_{track}$ and $\eta^{(l)}_{i,V^0} = \xi_i \zeta_{V^0}$, the results being $\zeta_{track} = 1.01 \pm 0.04$ and $\zeta_{V^0} = 1.03 \pm 0.07$, respectively.

The remaining entry in table 3 is the charged kaon-kaon correlation. Its contribution is small because kaon decay inside the jet chamber is unlikely due to the long kaon life time. Since

the charged and neutral kaon production rates are almost equal and the hyperon rates are much smaller than the kaon rates, the fraction F_{K^-,K^+} is close to 0.5 so that $\eta^{(a)}_{K^-,K^+} = \xi_{K^-}$.

In total, the contribution of all other sources to the observed correlation is smaller than the statistical error of the final result. Nevertheless, all sources were investigated in detail to minimize the systematic error.

A correlation potentially dangerous for the fit is the $\Sigma^-\mathrm{K}^+$ correlation. The corresponding asymmetry in table 2 is small, but actually it is the difference of much larger components. Strangeness conservation requires

$$F_{\Sigma^-,\overline{\Sigma^-}} + F_{\Sigma^-,\overline{\Sigma^+}} + 2\cdot F_{\Sigma^-,\overline{\Xi^-}} + 2\cdot F_{\Sigma^-,\overline{\Xi^0}} + F_{\Sigma^-,\overline{\Lambda}} + 2\cdot F_{\Sigma^-,K^+} \approx 1\ . \tag{10}$$

The parameters $F_{\Sigma^-,\overline{\Xi^-}}$ and $F_{\Sigma^-,\overline{\Xi^0}}$ appear with the weight 2 because the Ξ-particles carry two units of strangeness. The contribution from $\overline{\Omega^-}$ hyperons is negligible. The factor 2 in front of F_{Σ^-,K^+} accounts for the $\overline{\mathrm{K}^0}$ contribution, which cannot be measured. Monte Carlo simulations with different model parameters showed that relation (10) is fulfilled within 3%. Together with the condition for baryon number conservation,

$$F_{\Sigma^-,\overline{\Sigma^-}} + F_{\Sigma^-,\overline{\Sigma^+}} + F_{\Sigma^-,\overline{\Xi^-}} + F_{\Sigma^-,\overline{\Xi^0}} + F_{\Sigma^-,\overline{\Lambda}} + F_{\Sigma^-,\overline{p}} + F_{\Sigma^-,\overline{n}} \approx 1, \tag{11}$$

equation (10) gives the relation

$$F_{\Sigma^-,K^+} \approx \frac{1}{2}\cdot\left(F_{\Sigma^-,\overline{p}} + F_{\Sigma^-,\overline{n}} - F_{\Sigma^-,\overline{\Xi^-}} - F_{\Sigma^-,\overline{\Xi^0}}\right)\ , \tag{12}$$

which shows the presence of large compensating terms. In the analysis, F_{Σ^-,K^+} was therefore computed with the sum rule (10), taking the small correlations $F_{\Sigma^-,\overline{\Sigma^+}}$ and $F_{\Sigma^-,\overline{\Xi^0}}$ from the Monte Carlo generator. Similarly, F_{Ξ^-,K^+} can be constrained by the equivalent equation for the Ξ^-,

$$F_{\Xi^-,\overline{\Sigma^-}} + F_{\Xi^-,\overline{\Sigma^+}} + 2\cdot F_{\Xi^-,\overline{\Xi^-}} + 2\cdot F_{\Xi^-,\overline{\Xi^0}} + F_{\Xi^-,\overline{\Lambda}} + 2\cdot F_{\Xi^-,K^+} \approx 2\ . \tag{13}$$

The correlations of the Σ^+ hyperons are related to those of the Σ^- hyperon by the isospin symmetry, for instance $F_{\Sigma^+,\overline{\Lambda}} = F_{\Sigma^-,\overline{\Lambda}}$. No model independent predictions exist for $F_{K^-,\overline{\Lambda}}$ and the popcorn specific correlations $F_{\Sigma^-,\overline{\Xi^0}}$ and $F_{\Sigma^-,\overline{\Sigma^+}}$, which were determined with the Monte Carlo event sample.

The above relations allow either to replace $\eta^{(a)}_{i,k}$ by the four factors to be fitted, or to fix it and its contribution to the right hand side of equation (6). A simultaneous binned χ^2 fit, using equation (6), was performed for the d_0 distributions of the correlated-track and Λ candidates in the five $(m_{\Sigma^-}, \cos\theta^*)$-regions. In the Λ case, the reconstructed mass was restricted to the narrow interval given in section 2.5. In parallel, a fit of the like sign pairs to equation (5) was performed to determine $\zeta_{track} = \eta^{(l)}_{i,track}/\xi_i$ and three normalization factors for the hyperon-$\overline{\Lambda}$, K^--hyperon and (Σ^- or Ξ^-) – ($\overline{\Sigma^-}$ or $\overline{\Xi^-}$) correlations. The statistical errors of the pair rates, needed to compute χ^2, were computed with the equations (5) and (6); they depend on the result of the fit. The fit was therefore done iteratively, setting the unknown η-factors to unity for the first iteration. The statistical errors had d_0 dependent fluctuations due to

the limited Monte Carlo statistics. These were reduced with a one-dimensional smoothing algorithm described in [25]. The asymmetry fit resulted in a χ^2 value of 144 for 146 degrees of freedom. The coefficients obtained are correlated, the largest correlation coefficient being $\approx$-0.7 between $\eta^{(a)}_{\Sigma^-,\overline{\Sigma^-}}$ and $\eta^{(a)}_{\Sigma^-,\overline{\Xi^-}}$.

3.4 Experimental results and systematic errors

The adjusted d_0 distributions are shown in figs. 5 and 6. The histograms give the contributions of the correlated particle sources; all kink sources and two-dimensional bins j =*a,...e* are combined. The errors of the data points are statistical and the corresponding errors of the

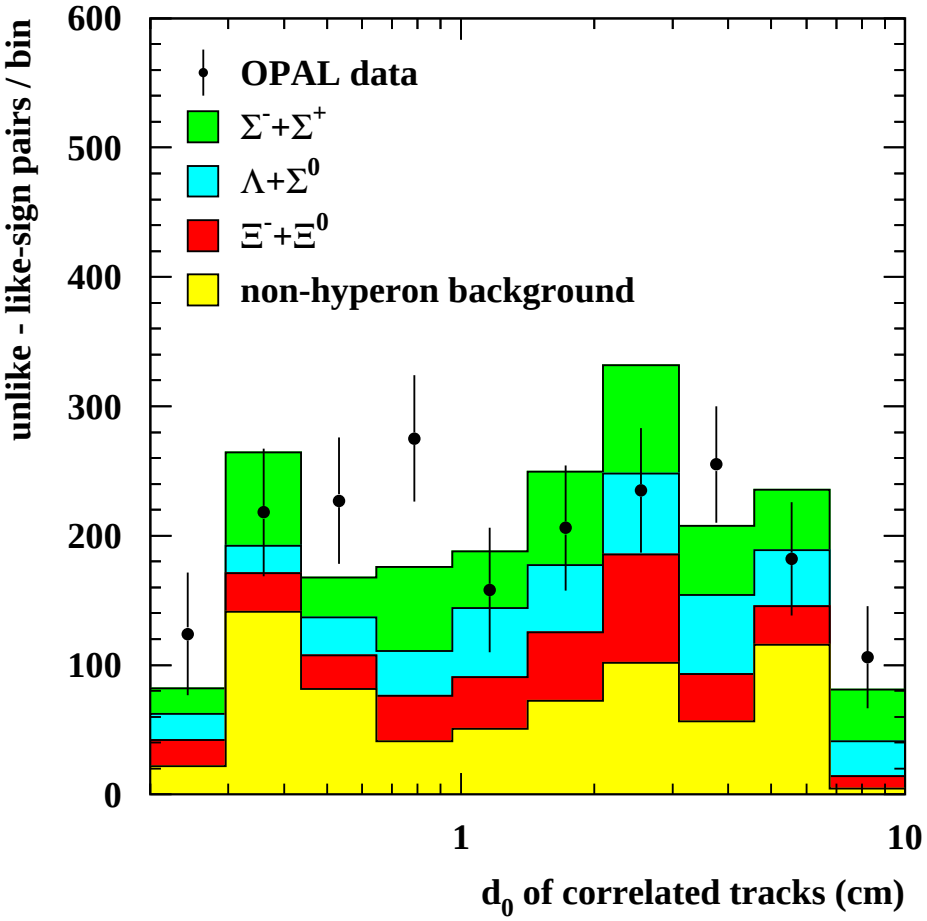

Figure 5: *Impact parameters of the displaced tracks, correlated to* Σ^- *candidates. The difference between unlike-sign and like-sign combinations is shown. Points: data. Histograms: results of the fit, ordered according to the sources for displaced tracks. The plotted errors are the statistical errors of the data.*

Monte Carlo histograms are not shown. Fig. 7 gives the rate differences between the unlike-sign and like-sign kink-V^0 pairs as a function of the reconstructed Λ mass. Both distributions are very well described.

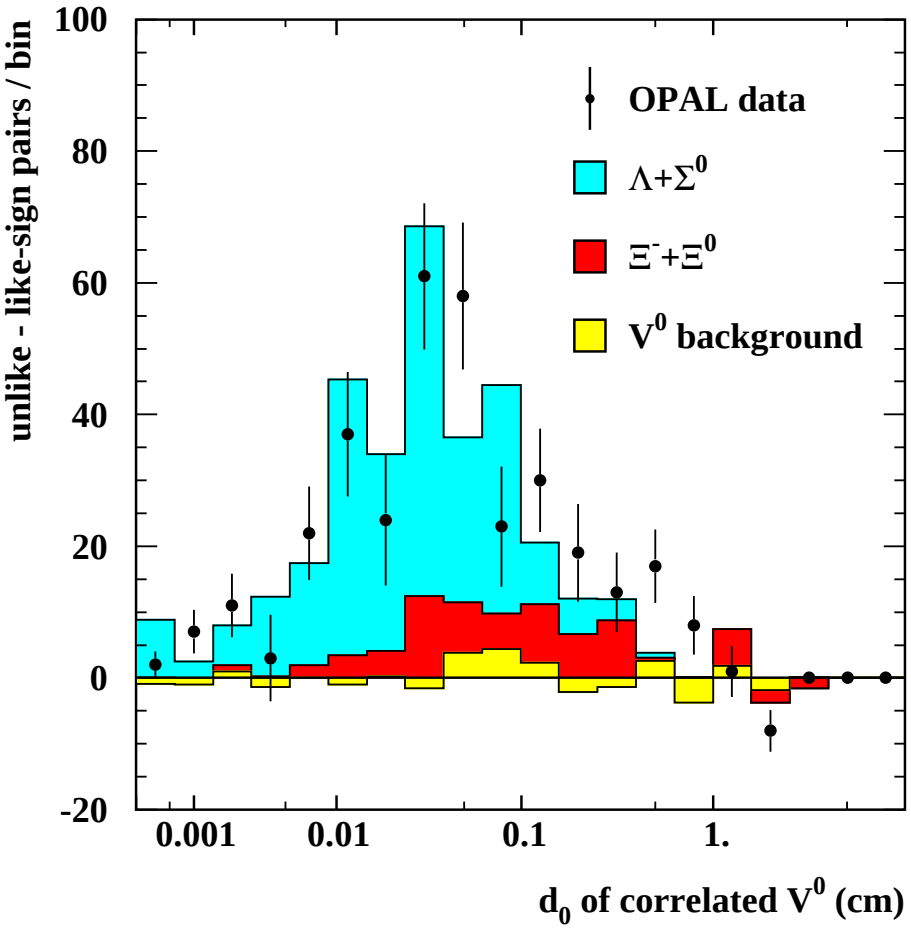

Figure 6: *Impact parameters of the $\overline{\Lambda}$ candidates, correlated to Σ^- candidates. The difference between unlike-sign and like-sign combinations is shown. Points: data. Histograms: results of the fit, ordered according to the V^0 sources. The plotted errors are the statistical errors of the data.*

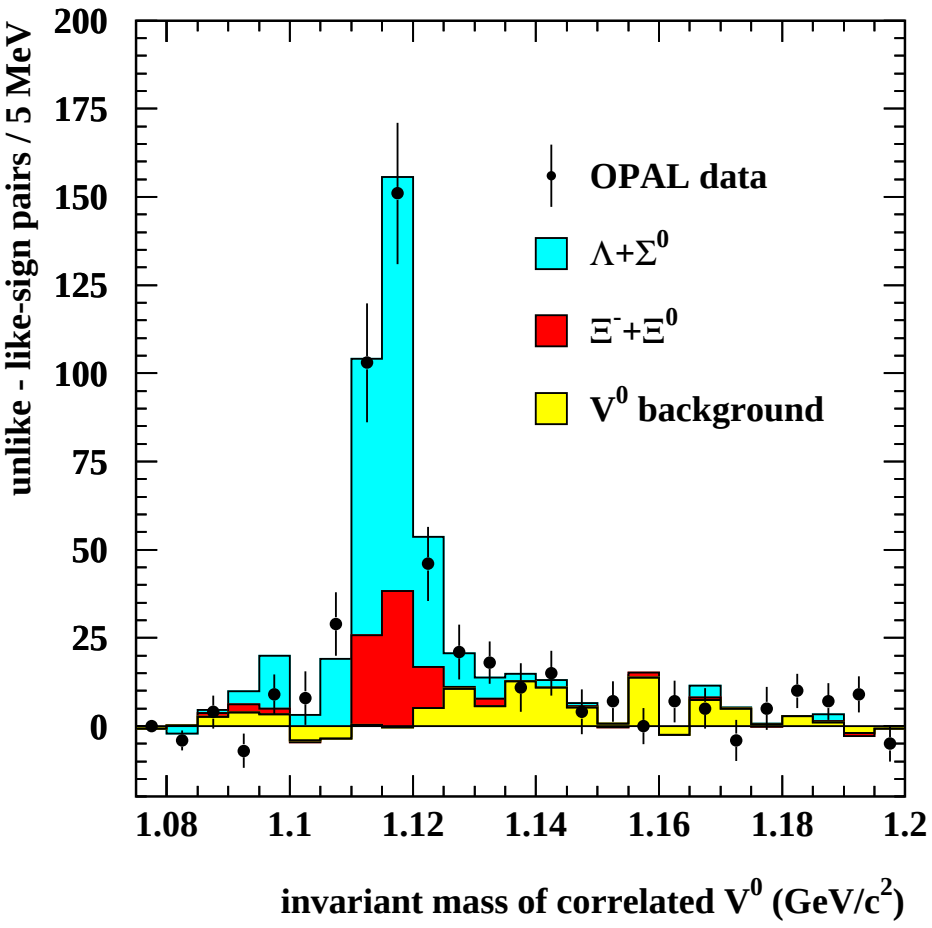

Figure 7: *Reconstructed masses of the* $\overline{\Lambda}$ *candidates, correlated to* Σ^- *candidates. The difference between unlike-sign and like-sign combinations is shown. Points: data. Histograms: results of the fit, ordered according to the* V^0 *sources. The plotted errors are the statistical errors of the data.*

	correlation			
	$F_{\Sigma^-,\overline{\Sigma^-}}$	$F_{\Sigma^-,\overline{\Xi^-}}$	$F_{\Sigma^-,\overline{\Lambda}}$	$F_{\overline{H}}$
fit result	0.162 ± 0.100	0.054 ± 0.047	0.234 ± 0.057	0.449 ± 0.091
systematic error				
mismodeling of correlated particle momenta	$+0.009$ ± 0.005	$+0.003$ ± 0.002	$+0.014$ ± 0.007	$+0.026$ ± 0.013
z-resolution at kink vertex	± 0.037	± 0.023	± 0.045	± 0.024
dE/dx calibration	± 0.010	± 0.005	± 0.004	± 0.008
hemisphere cut	± 0.005	± 0.002	± 0.007	± 0.013
number of hits per track	± 0.007	± 0.004	± 0.002	± 0.006
$\cos\theta$ distribution of tracks	± 0.012	± 0.001	± 0.001	± 0.012
Λ detection efficiency	± 0.006	± 0.004	± 0.004	± 0.002
charge asymmetry of detection efficiencies	± 0.002	± 0.001	± 0.001	± 0.002
uncertainty of popcorn channels	± 0.008	± 0.005	± 0.004	± 0.007
uncertainty of $\Xi^-\overline{\Xi^-}$ correlation	± 0.003	± 0.001	± 0.001	± 0.003
uncertainty of $\mathrm{K}^-\overline{\Lambda}$ correlation	± 0.001	± 0.001	± 0.003	± 0.002
final result	0.17 ± 0.11	0.057 ± 0.056	0.25 ± 0.08	0.48 ± 0.10

Table 5: *Experimental results and systematic errors.*

The fit results are listed in the first row of table 5. The errors are statistical and include the data and Monte Carlo contributions. Internally, the fit gets the Λ part of the correlation essentially from the correlated Λ sample, which sets also bounds on $F_{\Sigma^-,\overline{\Xi^-}}$. The $\Sigma^-\overline{\Sigma^-}$ correlation is computed from the displaced-track sample as a difference. Neither $F_{\Sigma^-,\overline{\Sigma^-}}$ nor $F_{\Sigma^-,\overline{\Xi^-}}$ differ from zero in a statistical way, in contrast to the overall sum $F_{\overline{H}}$. The smaller error of the sum is due to the strong anti-correlation between $F_{\Sigma^-\overline{\Sigma^-}}$ and $F_{\Sigma^-,\overline{\Xi^-}}$. The final results, including the systematic errors, are given in the last row of table 5.

The systematic errors, listed in table 5, will be discussed in the following.

Mismodeling of correlated particle momenta. The momentum spectra of the correlated pion and Λ candidates are not well reproduced by the Monte Carlo program. The simulated momenta have to be scaled downwards by as much as 20%. The effect exists both for the like sign and the unlike-sign track and V^0 candidates. As a consequence, the measured fractions $F_{i,\overline{k}}$ are systematically too small. To find a correction, the detection efficiencies for the correlated particles were extracted from the Monte Carlo sample and the shifted momentum spectrum was folded with the efficiency function. This leads to an upwards correction of the measured correlations. A global correction of $(6 \pm 3)\%$ was applied. This correction, together with its error, is much larger than the uncertainties

due to miscalibrations of the particle momenta or the impact parameters. Therefore, no additional errors were assigned to the momentum and d_0 selection cuts.

z-resolution at kink vertex. In the ratio of a correlated rate to the single Σ^- rate the overall detection efficiency for Σ^- hyperons cancels. However, an uncertainty of the number of observed Σ^- hyperons arises from the unfolding procedure. The dominating error source is the mismodeling of the z-resolution. The correction factor c, introduced above, was conservatively varied between 1.25 and 1.5. For the individual correlations $F_{\Sigma^-,\overline{k}}$ the obtained shifts were found to be non-parabolic functions of c. The maximal shifts of the results $F_{\Sigma^-,\overline{k}}$ and $F_{\overline{H}}$ were taken as uncertainties.

dE/dx calibration. Any antiproton impurity in the displaced track sample reduces the asymmetry from direct or indirect $\overline{\Lambda}$ decays. For a pure pion sample and a perfect calibration, the frequency distribution of the weight $w_{dE/dx}(\pi)$, defined in section 2.4, should not depend on $w_{dE/dx}(\pi)$. A superimposed peak at $w_{dE/dx}(\pi) = 0$ is expected due to non-pions. The shape of this peak does not perfectly agree with the Monte Carlo prediction. A systematic error was assigned to the corresponding mismodeling of the antiproton rejection efficiency.

Hemisphere cut. In principle, the results are corrected automatically for the hemisphere cut. No significant correlations were observed in the dropped hemisphere. A systematic error would appear, if the fragmentation model were incorrect. A 3% error was assigned to all correlations, based on the error of the number of tracks in the omitted hemisphere.

Other systematic errors The number of hits per track is well modeled and introduces an error of 1% for the number of displaced tracks. Also the acceptance cut for the θ angle plays a minor role only. From the difference between the angular distributions of data and Monte Carlo events an efficiency error of 3% was estimated. Systematic errors due to the cuts for Λ selection were already discussed in [21]. An uncertainty of $\pm 3.3\%$ was taken from that paper as fully correlated error for the Λ event sample. Differences $\Delta\epsilon_i$ between the detection efficiencies for particles and antiparticles would lead to a spurious asymmetry, if both the kinks i and the correlated particles k are affected. The effect is proportional to $\Delta\epsilon_{\Sigma^-} \cdot \Delta\epsilon_k$. The efficiency differences were extracted from the observed particle and antiparticle rates and the upper limits for the spurious asymmetries in table 5 were obtained. Furthermore, there are uncertainties due to the model dependence of the correlations which had to be subtracted. One half of the Monte Carlo baryon antibaryon pairs are accompanied by a popcorn meson. The $\eta^{(a)}$-factors for the popcorn specific correlations $\Sigma^-\overline{\Sigma^+}$, $\Sigma^-\overline{\Xi^0}$ and $\Xi^-\overline{\Sigma^+}$ were varied between 0 and 2 and the fit repeated. The $\mathrm{K}^-\overline{\Lambda}$ correlation was varied by 50% and an uncertainty of 20% was assigned to the $\Xi^-\overline{\Xi^-}$ correlation, fixing the small residual contribution from Ξ^- self correlations. As already mentioned, the definition of $F_{\overline{H}}$ introduces a small amount of double counting, both in the data and in the Monte Carlo simulation. This problem was studied with a toy Monte Carlo program and the only effects found were negligible corrections to the statistical errors of the fit.

The correlated kink-track and kink-V^0 pairs should be concentrated in the Σ^- enriched bins a and d in the $(m_{\Sigma^-}, \cos\theta^*)$ plane shown in figure 2. As a cross check, a simpler analysis was performed, where the analysis was restricted to region a. All background asymmetries

and also the $\Xi^-\overline{\Lambda}$ correlation were subtracted as predicted by the Monte Carlo program. The final result including reevaluated systematic errors, $F_{\overline{H}} = 0.472 \pm 0.155$, is fully consistent with the main result and demonstrates the absence of anomalies in the $(m_{\Sigma^-}, \cos\theta^*)$ plane.

4 Comparison with fragmentation models

Before comparing the result for $F_{\overline{H}}$ to the predictions of models, we adjusted the models, incorporated into the PYTHIA Monte Carlo event generator, to describe a set of observables in Z^0 decays. The optimization began with the PYTHIA steering parameters given in [24]. These were slightly modified to reproduce the newest experimental information on the baryonic sector, including data on $\Lambda\overline{\Lambda}$ correlations. The tuned Monte Carlo was then used to predict $F_{\overline{H}}$. We also used the models to study $p\pi\overline{p}$ correlations more extensively than previously, as described below.

4.1 Observables

The input observables for the tuning fall into four categories:

1. Eight baryon multiplicities in multihadronic Z^0 decay: p, Δ^{++}, Λ, $\Sigma^+ + \Sigma^-$, Σ^0, Ξ^-, $\Sigma^{*+} + \Sigma^{*-}$, and Ω^-. The production rates were taken from the compilation of the particle data group [14].

2. Proton and Λ momentum spectra. Baryon spectra have approximately Gaussian shapes if parameterized in terms of the variable $\xi = \ln(1/x_p)$ [1]. We use the mean values and variances of the proton and Λ spectra as the observables. Deviations from the normal distribution are known, the true maxima being somewhat higher than the result of the fit [27, 31]. However, the Gaussian fit is an easy way to compare different experiments. The tabulated data [27]–[31] were fitted to Gaussian functions in the interval $1.2 < \xi < 4.2$. The situation for the protons is not satisfactory, the fitted maxima of the ξ distributions varying from 2.79 [28] to 3.08 [31]. The values $\xi_{peak} = 2.80 \pm 0.07$ and $\sigma = 1.11 \pm 0.06$ were obtained with a combined fit using all LEP and SLD data. The errors were not taken from the fit but conservatively estimated from the systematic differences between the ξ spectra of the experiments. It should be noted that both ξ_{peak} and σ depend on the fit range due to deviations of the ξ-distribution from the Gaussian shape. The agreement between experiments is better for Λ production, leading to values $\xi_{peak} = 2.62 \pm 0.04$ and $\sigma = 1.21 \pm 0.04$.

3. $\Lambda\overline{\Lambda}$ correlations. The correlation was parameterized by two observables, the first one being the rate excess of $\Lambda\ \overline{\Lambda}$ pairs over $\Lambda\ \Lambda\ +\ \overline{\Lambda}\ \overline{\Lambda}$ pairs per event, $N^{corr}_{\Lambda\overline{\Lambda}}$. The other observable is the mean rapidity difference $\overline{\Delta y}_{\Lambda\overline{\Lambda}}$ between the Λ and $\overline{\Lambda}$ after subtraction of like-sign pairs. The number of correlated $\Lambda\ \overline{\Lambda}$ pairs per event was taken from [12]. The mean $\Lambda\overline{\Lambda}$ rapidity difference $\overline{\Delta y}$ was computed from the data of [12], as the truncated mean for $\Delta y < 3.0$. This cut was introduced to suppress the contribution of Λ's from the opposite event hemisphere.

4. Nine meson production rates per multihadronic Z^0 decay: $\pi^+ + \pi^-$, π^0, $K^+ + K^-$, K^0_S, $\rho^+ + \rho^-$, ρ^0, φ, $K^{*+}(892) + K^{*-}(892)$ and $K^{*0}(892)$. These rates, taken from [14], were included in the tuning to protect the meson generation against parameter modifications steering the baryonic sector.

4.2 Model Parameters

The popcorn mechanism is incorporated in PYTHIA in two ways [9]. The first **simple version** was originally introduced in JETSET. Baryon production is controlled by the following parameters:

1. the suppression of diquark-antidiquark production relative to quark-antiquark production, $\mathbf{P}(qq)/\mathbf{P}(q)$ = PARJ(1);
2. the suppression of $s\overline{s}$ production relative to $u\overline{u}$ production, $\mathbf{P}(s)/\mathbf{P}(u)$ = PARJ(2); a tuning of this parameter was necessary, because the strange meson rates had to be readjusted;
3. a double ratio involving diquarks containing s quarks, $(\mathbf{P}(us)/\mathbf{P}(ud))/(\mathbf{P}(s)/\mathbf{P}(u))$ = PARJ(3);
4. the suppression factor for spin 1 diquarks, $(1/3)\mathbf{P}(ud_1)/\mathbf{P}(ud_0)$ = PARJ(4);
5. the popcorn parameter, which determines the relative occurrences of the baryon-meson-antibaryon and baryon-antibaryon configurations, PARJ(5);
6. an extra suppression for having an $s\ \overline{s}$ pair in a baryon-meson-antibaryon configuration, PARJ(6);
7. an extra suppression for having a strange meson in a baryon-meson-antibaryon configuration, PARJ(7);
8. a parameter which enters the exponent of the Lund symmetric fragmentation function for diquarks, PARJ(45); this parameter has an impact on the rapidity difference in baryon-antibaryon correlations.

In the **advanced popcorn** scheme, a universal equation for tunneling from the vacuum is applied to the generation of new partons and an arbitrary number of mesons can be created between a baryon and an antibaryon. The tunneling probability is proportional to $\exp(-\beta_q \cdot M_\perp)$, where β_q is a flavor dependent model parameter and $M_\perp$ the transverse mass of the created object. Only the first two and the last parameter of the above list are used in this scheme. There are three new parameters, two of them related to the tunneling formula:

9. the tunneling coefficient for u-quarks, β_u = PARJ(8);
10. $\delta\beta = \beta_s - \beta_u$ = PARJ(9)
11. an extra suppression factor for spin 3/2 baryons = PARJ(18).

popcorn parameter PARJ(5)		0.	0.5	1.	5.	
observable	data	MC1	MC2	MC3	MC4	MC5 advanced popcorn
χ^2	-	56	59	59	63	99
$N^{corr}_{\Lambda\overline{\Lambda}}$	0.0612 ± 0.0034	0.066	0.060	0.066	0.058	0.081
$\overline{\Delta y}_{\Lambda\overline{\Lambda}}$	0.71 ± 0.04	0.66	0.69	0.67	0.75	0.57
$F_{\Sigma^-,\overline{\Sigma^-}}$ (this work)	0.17 ± 0.11	0.39	0.34	0.30	0.19	0.20
$F_{\Sigma^-,\overline{\Xi^-}}$ (this work)	0.057 ± 0.056	0.18	0.16	0.15	0.09	0.08
$F_{\Sigma^-,\overline{\Lambda}}$ (this work)	0.25 ± 0.08	0.30	0.28	0.28	0.27	0.28
$F_{\overline{H}}$ (this work)	0.48 ± 0.10	0.87	0.79	0.73	0.55	0.56

Table 6: *Comparison with fragmentation models. Fit quality χ^2, $\Lambda\overline{\Lambda}$ correlations and the Σ^- antihyperon correlations as defined in the text. The errors of the simulation are smaller than the last digit shown.*

4.3 Simulation Results

For a given PYTHIA parameter set, the measured observables from section 4.1 were compared with the simulation results and a χ^2 was computed. It cannot be expected from a fragmentation model that all its predictions are correct to better than a few percent. To reduce the contributions of very accurately measured observables, the errors to compute χ^2 were thus taken to be at least 2.5%, which represents the characteristic level of agreement between the data and MC. Low χ^2 values were searched for with the method described in the appendix, for fixed values of the popcorn parameter. Many tunes of the generator have almost the same quality. Some PYTHIA parameter sets and the predicted baryon production rates are given in the appendix. Table 6 shows the χ^2's, the $\Lambda\overline{\Lambda}$ correlations and the Σ^--antihyperon correlations, as a function of the popcorn parameter, where the simple popcorn model is denoted MC1 to MC4.

The variable χ^2 is an indicator for the quality of the baryon modeling. For the simple popcorn model, the lowest χ^2 value found was 56 for the 23 observables. This means that the Monte Carlo generator describes, on average, the observables roughly within 2 times the experimental errors or 5%, whichever is larger.

The most important result of the simulation is that the overall quality of the description of the observables does not depend strongly on the popcorn parameter in the simple popcorn model. The $\Lambda\overline{\Lambda}$ correlation parameters are always reproduced within two standard deviations, whether the popcorn effect is switched on or off. The Monte Carlo parameter space examined here is larger than that in earlier studies. In view of the overall uncertainty it is not possible to reach a definite conclusion about the the popcorn effect by using $\Lambda\overline{\Lambda}$ correlations.

As shown in the bottom line of table 6, the measured fraction $F_{\overline{H}}$ is consistent both with the predictions of the original popcorn model with a large popcorn parameter (MC4) and the

optimized advanced popcorn model (MC5), but is smaller than the Monte Carlo prediction for zero popcorn effect. It was investigated whether models without the popcorn mechanism could be found that reproduce the observables of section 4.1 and give $F_{\overline{H}} \ll 0.9$. The relevant parameters of the PYTHIA generator from section 4.2, including the diquark fragmentation function, were randomly varied as described in the appendix. In these studies, $F_{\overline{H}}$ values less than 0.86 were not obtained. The experimental result deviates from this lower limit by 3.8 standard deviations.

The advanced popcorn model has fewer parameters available for tuning and provides a significantly worse description of data as seen from the larger χ^2 value. The larger χ^2 for this model arises to a large extent from two well known facts. The absolute number of $\Lambda\ \overline{\Lambda}$ pairs is too large and the distribution of the $\Lambda\ \overline{\Lambda}$ rapidity differences is too narrow in comparison to the observation [12]. On the other hand, the average $\Lambda\overline{\Lambda}$ rapidity difference in the simple popcorn model with a very large popcorn parameter is too large, so that a combination of the two models might possibly describe the $\Lambda\overline{\Lambda}$ correlation well.

To complete the comparison of correlations with results from Monte Carlo generators, the DELPHI $\mathrm{p}\pi\overline{\mathrm{p}}$ [13] correlation was also investigated. This was done for rapidity ordered $\mathrm{p}\pi\overline{\mathrm{p}}$ and $\pi\mathrm{p}\overline{\mathrm{p}}$ or $\mathrm{p}\overline{\mathrm{p}}\pi$ particle configurations inside event hemispheres. The selection cuts and the definition of the minimum rapidity gap Δy_{min} between a selected pion and the next proton were taken from [13]. The discriminating variable of [13] is the ratio of intensities

$$R(\Delta y_{min}) = \frac{N(\mathrm{p}\pi\overline{\mathrm{p}})}{N(\mathrm{p}\pi\overline{\mathrm{p}}) + N(\pi\mathrm{p}\overline{\mathrm{p}} + \mathrm{p}\overline{\mathrm{p}}\pi)} \tag{14}$$

at the rapidity difference Δy_{min}. A strong dependence on the popcorn effect had been seen by [13] at large values of Δy_{min}. For three bins in the range $0.625 \leq \Delta y_{min} \leq 1$, the observed distribution agreed with a subsample of Monte Carlo events without the popcorn mechanism and disagreed with a disjunct subsample, containing popcorn mesons, by more than five standard deviations, averaged over the three bins.

These results could be reproduced with the simulations described here: The R distributions obtained with the parameter set MC1, but without detector corrections, agreed with DELPHI's observation within 1.9 standard deviations, while there was disagreement between the data and Monte Carlo study MC2 by 5.2 standard deviations, averaged over the same three Δy_{min} bins. Variations of the fragmentation model had not been studied in [13]. An increase of the fragmentation parameter PARJ(45) to unity, fixing the other parameters of the simulation MC2, reduces the difference between the data and the model prediction to 2.4 standard deviations. Furthermore, it was found that the advanced popcorn model with the parameter set MC5 results in almost the same function $R(\Delta y_{min})$ as the model MC1 without the popcorn effect.

The modification of the parameter PAR(45) in the simulation MC2 increased the χ^2 value in table 6 from 59 to 70 due to a shift of $\overline{\Delta y}_{\Lambda\overline{\Lambda}}$ to a value below the observation, without degrading the description of the other observables of section 4.1. In summary, these results indicate a high sensitivity of the rapidity correlations to the fragmentation dynamics.

popcorn parameter PARJ(5)		0.	0.5	1.	5.	
observable	data	MC1	MC2	MC3	MC4	MC5 advanced popcorn
protons	1.046 ± 0.026	1.03	1.03	1.02	1.09	1.01
Δ^{++}	0.087 ± 0.033	0.098	0.118	0.122	0.122	0.127
Λ	0.388 ± 0.009	0.369	0.362	0.366	0.388	0.388
$\Sigma^+ + \Sigma^-$	0.181 ± 0.018	0.129	0.131	0.129	0.133	0.141
Σ^0	0.076 ± 0.010	0.069	0.070	0.069	0.070	0.073
Ξ^-	0.0258 ± 0.0009	0.029	0.029	0.028	0.029	0.024
$\Sigma^*(1385)^{+,-}$	0.046 ± 0.004	0.043	0.048	0.052	0.051	0.054
Ω^-	0.0016 ± 0.0003	0.0005	0.0004	0.0004	0.0004	0.0004

Table 7: *Baryon rates per multihadronic event. The errors of the simulation are smaller than the last digit shown.*

5 Conclusions

Our investigations indicate that the fragmentation models have not yet reached a state where they can quantitatively describe the $\Lambda\overline{\Lambda}$ correlations, the $p\overline{p}\pi$ correlations and the Σ^- antihyperon correlation $F_{\overline{H}}$ simultaneously. Neither the $\Lambda\overline{\Lambda}$ nor the $p\overline{p}\pi$ correlations can provide a clear conclusion about the popcorn effect because they can both be described to an acceptable level by models either with and without the popcorn mechanism. The PYTHIA generator without the popcorn effect can reproduce both rapidity correlations simultaneously within two standard deviations. Both correlations are also in acceptable agreement with model predictions including the popcorn effect. However, we were unable to find a variant of the popcorn model that could simultaneously describe both types of correlations.

In this work, the mechanism of baryon formation was studied by counting Σ^- hyperons and correlated antihyperons from hadronic Z^0decays. The result $F_{\overline{H}} = 0.48 \pm 0.10$, based on data taken by the OPAL experiment at LEP, favors a large popcorn parameter in the simple popcorn model and is also consistent with the advanced popcorn model. The fragmentation dynamics play no role here because the rapidity is not used in the analysis. Correlated particle momenta play an indirect role only, because they influence the detection efficiencies, but the final result contains a correction and a systematic error for mismodeling.

Trivial correlations between hyperons and antihyperons based on baryon number and strangeness conservation, as predicted by the thermodynamic model, always exist. Due to the limited data statistics and the insensitivity to the dynamics, our result gives only a weak indication for non-trivial quark correlations between baryon-antibaryon pairs. Statistical models, only constrained by conservation laws, differ at most by 2.6 standard deviations.

The result for $F_{\overline{H}}$ deviates from the lower limit of simulations without the popcorn effect by 3.8 standard deviations and thus demonstrates the need for the the popcorn effect in order to reproduce baryon correlations within the diquark fragmentation model, where a baryon

model parameter	standard OPAL tune	MC1	MC2	MC3	MC4	MC5 advanced popcorn
PARJ(5)	0.5	0.	0.5	1.	5.	-
PARJ(1)	0.085	0.092	0.100	0.101	0.117	0.226
PARJ(2)	0.31	0.33	0.33	0.34	0.34	0.31
PARJ(3)	0.45	0.32	0.41	0.40	0.48	-
PARJ(4)	0.025	0.055	0.029	0.021	0.007	-
PARJ(6)	0.5	-	0.33	0.56	0.35	-
PARJ(7)	0.5	-	0.21	0.20	0.28	-
PARJ(8)	-	-	-	-	-	1.00
PARJ(9)	-	-	-	-	-	2.07
PARJ(18)	-	-	-	-	-	0.18
PARJ(45)	0.5	0.16	0.22	0.52	0.33	0.27

Table 8: *Parameter sets used for the simulations in tables 6 and 7.*

MC parameter	PARJ(1)	PARJ(2)	PARJ(3)	PARJ(4)	PARJ(45)
mean value	0.091	0.31	0.35	0.045	0.50
interval	± 0.008	± 0.04	± 0.08	± 0.012	± 0.50

Table 9: *Parameter ranges used for random generation of Monte Carlo parameter sets without the popcorn effect.*

and an antibaryon share two valence quark-antiquark pairs. More generally, one expects any fragmentation model with very strong valence quark correlations between baryons and antibaryons to be disfavored.

Appendix: Tuning of the Monte Carlo generator

The tuning started with the PYTHIA parameters of [24], listed as "standard OPAL tune" in table 8. In a first step, the parameters, except the popcorn parameter, were varied individually and minimum values of χ^2 were searched for. This process was iterated. Search ranges for all parameters were defined either by requiring a maximum increase in χ^2 of 20 or, in the case of smaller changes, by allowing a parameter shift of $\pm 100\%$. Finally, all parameters were varied randomly within these ranges to search for χ^2 values lower than that of the solution already found. Between 200 and 300 random parameter sets were generated at fixed PARJ(5) for the final search and 10^5 events were generated per parameter set. The results for the selected parameters sets MC1 to MC5 are based on 10^6 events. The contributions of the four classes of observables to χ^2 at the minimum value 56 are about 40 from the baryon rates, 10 from the meson rates and 6 from the remaining six observables.

The measured and simulated baryon rates per Z^0 decay are given in table 7, while the corresponding PYTHIA parameters are listed in table 8. The Ω^- baryon was included in

the optimization to avoid its almost complete suppression. The results for the parameter sets MC3 and MC5 are similar to those in our previous publication [12], where the case without the popcorn effect was not investigated. The reproduction of the meson sector does not change much during the tuning and is therefore omitted from table 7.

Finally, table 9 gives the parameter space for the study of the parameter dependence of $F_{\overline{H}}$. All cases with $\chi^2 < 110$ were kept, allowing average discrepancies between the data and the model as large as those obtained with the modified popcorn model.

Acknowledgments

We are grateful to F.Becattini for applying the thermodynamic model to the Σ^- antihyperon correlations and we thank J.Lamsa and K.Hamacher from the DELPHI collaboration for discussions about the proton-antiproton-pion correlations. We particularly wish to thank the SL Division for the efficient operation of the LEP accelerator at all energies and for their close cooperation with our experimental group. In addition to the support staff at our own institutions we are pleased to acknowledge the
Department of Energy, USA,
National Science Foundation, USA,
Particle Physics and Astronomy Research Council, UK,
Natural Sciences and Engineering Research Council, Canada,
Israel Science Foundation, administered by the Israel Academy of Science and Humanities,
Benoziyo Center for High Energy Physics,
Japanese Ministry of Education, Culture, Sports, Science and Technology (MEXT) and a grant under the MEXT International Science Research Program,
Japanese Society for the Promotion of Science (JSPS),
German Israeli Bi-national Science Foundation (GIF),
Bundesministerium für Bildung und Forschung, Germany,
National Research Council of Canada,
Hungarian Foundation for Scientific Research, OTKA T-038240, and T-042864,
The NWO/NATO Fund for Scientific Research, the Netherlands.

References

[1] Y. L. Dokshitzer, V. A. Khoze, S. I. Troyan, Z. Phys. **C55** (1992) 107;
Int. J. Mod. Phys. **A7** (1992) 1875.

[2] F. Becattini, Z. Phys. **C69** (1996) 485;
J. Phys. **G23** (1997) 1933.

[3] G. Marchesini *et al.*, Comp. Phys. Comm. **67** (1992) 465.

[4] B. Andersson, G. Gustafson, G. Ingelman and T. Sjöstrand, Phys. Rep. **97** (1983) 31.

[5] B. Andersson, G. Gustafson and T. Sjöstrand, Nucl. Phys. **B197** (1982) 45.

[6] B. Andersson, G. Gustafson and T. Sjöstrand, Phys. Scripta **32** (1985) 574.

[7] P. Eden and G. Gustafson, Z. Phys. **C75** (1997) 41.

[8] T. Sjöstrand, Comp. Phys. Comm. **92** (1994) 74.

[9] T. Sjöstrand *et al.*, Comp. Phys. Comm. **135** (2001) 238.

[10] ALEPH Collaboration, D. Busculic *et al.*, Z. Phys. **C64** (1994) 361.

[11] DELPHI Collaboration, P. Abreu *et al.*, Phys. Lett. **B416** (1998) 247;
DELPHI Collaboration, P. Abreu *et al.*, Phys. Lett. **B318** (1993) 249.

[12] OPAL Collaboration, G. Abbiendi *et al.*, Eur. Phys. J. **C13** (2000) 185;
OPAL Collaboration, P. Acton *et al.*, Phys. Lett. **B305** (1993) 415.

[13] DELPHI Collaboration, P. Abreu *et al.*, Phys. Lett. **B490** (2000) 61.

[14] Review of Particle Properties, C. Amsler *et al.*(Particle Data Group), Phys. Lett. **B669** (2008) 1.

[15] F. Becattini and G. Passaleva, Eur. Phys. J. **23** (2002) 551;
F. Becattini, private communication.

[16] OPAL Collaboration, K. Ahmet *et al.*, Nucl. Instr. Meth. **A305** (1991) 275.

[17] P. Allport *et al.*, Nucl. Instr. Meth. **A324** (1993) 34;
P. Allport *et al.*, Nucl. Instr. Meth. **A346** (1994) 476.

[18] O. Biebel *et al.*, Nucl. Instr. Meth. **323** (1992) 169.

[19] OPAL Collaboration, G. Alexander *et al.*, Z. Phys. **C52** (1991) 175.

[20] OPAL collaboration, G. Alexander *et al.*, Z. Phys. **C73** (1997) 587.

[21] OPAL collaboration, G. Alexander *et al.*, Z. Phys. **C73** (1997) 569;
OPAL Collaboration, P. D. Acton *et al.*, Phys. Lett. **B291** (1992) 503.

[22] J. Allison *et al.*, Nucl. Instr. Meth. **A317** (1992) 47.

[23] OPAL Collaboration, P. D. Acton *et al.*, Z. Phys. **C58** (1993) 387.

[24] OPAL Collaboration, G. Alexander *et al.*, Z. Phys. **C69** (1996) 543.

[25] P. Bock, JHEP **08** (2006) 56.

[26] M. Hauschild *et al.*, Nucl. Instr. Meth. **A314** (1992) 74.

[27] DELPHI Collaboration, P. Abreu *et al.*, Eur. Phys. J. **C5** (1998) 585.

[28] ALEPH Collaboration, R. Barate *et al.*, Eur. Phys. J. **C5** (1998) 205;
ALEPH Collaboration, Phys. Rep. **204** (1998) 1.

[29] OPAL Collaboration, R. Akers etal, Z. Phys. **C63** (1994) 181.

[30] ALEPH Collaboration, R. Barate *et al.*, Eur. Phys. J. **C16** (2000) 613;
L3 Collaboration, M. Acciari *et al.*, Phys. Lett. **B407** (1997) 389;
DELPHI Collaboration, P. Abreu *et al.*, Phys. Lett. **318** (1993) 249.

[31] SLD Collaboration, K. Abe *et al.*, Phys. Rev. **D69** (2004) 072003.

EUROPEAN ORGANIZATION FOR NUCLEAR RESEARCH

CERN-PH-EP/2009-XXX
May 14, 2009

Σ^--antihyperon correlations in Z^0 decay and investigation of the baryon production mechanism

The OPAL Collaboration

Abstract

Data collected around $\sqrt{s}$ =91 GeV by the OPAL experiment at the LEP e^+e^- collider are used to study the mechanism of baryon formation. As the signature, the fraction of Σ^- hyperons whose baryon number is compensated by the production of a $\overline{\Sigma^-}$, $\overline{\Lambda}$ or $\overline{\Xi^-}$ antihyperon is determined. The method relies entirely on quantum number correlations of the baryons, and not rapidity correlations, making it more model independent than previous studies. The diquark fragmentation model without the popcorn mechanism is strongly disfavored with a significance of 3.8 standard deviations including systematic uncertainties. It is shown that previous studies of the popcorn mechanism are not conclusive if parameter uncertainties are considered.

(To be submitted to Eur. Phys. J. C.)

The OPAL Collaboration

G. Abbiendi[2], C. Ainsley[5], P.F. Åkesson[7], G. Alexander[21], G. Anagnostou[1], K.J. Anderson[8], S. Asai[22], D. Axen[26], I. Bailey[25], E. Barberio[7,p], T. Barillari[31], R.J. Barlow[15], R.J. Batley[5], P. Bechtle[24], T. Behnke[24], K.W. Bell[19], P.J. Bell[1], G. Bella[21], A. Bellerive[6], G. Benelli[4], S. Bethke[31], O. Biebel[30], O. Boeriu[9], P. Bock[10], M. Boutemeur[30], S. Braibant[2], R.M. Brown[19], H.J. Burckhart[7], S. Campana[4], P. Capiluppi[2], R.K. Carnegie[6], A.A. Carter[12], J.R. Carter[5], C.Y. Chang[16], D.G. Charlton[1], C. Ciocca[2], A. Csilling[28], M. Cuffiani[2], S. Dado[20], M. Dallavalle[2], A. De Roeck[7], E.A. De Wolf[7,s], K. Desch[24], B. Dienes[29], J. Dubbert[30], E. Duchovni[23], G. Duckeck[30], I.P. Duerdoth[15], E. Etzion[21], F. Fabbri[2], P. Ferrari[7], F. Fiedler[30], I. Fleck[9], M. Ford[15], A. Frey[7], P. Gagnon[11], J.W. Gary[4], C. Geich-Gimbel[3], G. Giacomelli[2], P. Giacomelli[2], M. Giunta[4], J. Goldberg[20], E. Gross[23], J. Grunhaus[21], M. Gruwé[7], A. Gupta[8], C. Hajdu[28], M. Hamann[24], G.G. Hanson[4], A. Harel[20], M. Hauschild[7], C.M. Hawkes[1], R. Hawkings[7], G. Herten[9], R.D. Heuer[24], J.C. Hill[5], D. Horváth[28,c], P. Igo-Kemenes[a1], K. Ishii[22], H. Jeremie[17], P. Jovanovic[1], T.R. Junk[6,i], J. Kanzaki[22,u], D. Karlen[25], K. Kawagoe[22], T. Kawamoto[22], R.K. Keeler[25], R.G. Kellogg[16], B.W. Kennedy[19], S. Kluth[31], T. Kobayashi[22], M. Kobel[3,t], S. Komamiya[22], T. Krämer[24], A. Krasznahorkay Jr.[29,e], P. Krieger[6,l], J. von Krogh[10], T. Kuhl[24], M. Kupper[23], G.D. Lafferty[15], H. Landsman[20], D. Lanske[13], D. Lellouch[23], J. Letts[o], L. Levinson[23], J. Lillich[9], S.L. Lloyd[12], F.K. Loebinger[15], J. Lu[26,b], A. Ludwig[3,t], J. Ludwig[9], W. Mader[3,t], S. Marcellini[2], A.J. Martin[12], T. Mashimo[22], P. Mättig[m], J. McKenna[26], R.A. McPherson[25], F. Meijers[7], W. Menges[24], F.S. Merritt[8], H. Mes[6,a], N. Meyer[24], A. Michelini[2], S. Mihara[22], G. Mikenberg[23], D.J. Miller[14], W. Mohr[9], T. Mori[22], A. Mutter[9], K. Nagai[12], I. Nakamura[22,v], H. Nanjo[22], H.A. Neal[32], S.W. O'Neale[1,*], A. Oh[7], M.J. Oreglia[8], S. Orito[22,*], C. Pahl[31], G. Pásztor[4,g], J.R. Pater[15], J.E. Pilcher[8], J. Pinfold[27], D.E. Plane[7], O. Pooth[13], M. Przybycień[7,n], A. Quadt[31], K. Rabbertz[7,r], C. Rembser[7], P. Renkel[23], J.M. Roney[25], A.M. Rossi[2], Y. Rozen[20], K. Runge[9], K. Sachs[6], T. Saeki[22], E.K.G. Sarkisyan[7,j], A.D. Schaile[30], O. Schaile[30], P. Scharff-Hansen[7], J. Schieck[31], T. Schörner-Sadenius[7,z], M. Schröder[7], M. Schumacher[3], R. Seuster[13,f], T.G. Shears[7,h], B.C. Shen[4], P. Sherwood[14], A. Skuja[16], A.M. Smith[7], R. Sobie[25], S. Söldner-Rembold[15], F. Spano[8,x], A. Stahl[13], D. Strom[18], R. Ströhmer[30], S. Tarem[20], M. Tasevsky[7,d], R. Teuscher[8], M.A. Thomson[5], E. Torrence[18], D. Toya[22], I. Trigger[7,w], Z. Trócsányi[29,e], E. Tsur[21], M.F. Turner-Watson[1], I. Ueda[22], B. Ujvári[29,e], C.F. Vollmer[30], P. Vannerem[9], R. Vértesi[29,e], M. Verzocchi[16], H. Voss[7,q], J. Vossebeld[7,h], C.P. Ward[5], D.R. Ward[5], P.M. Watkins[1], A.T. Watson[1], N.K. Watson[1], P.S. Wells[7], T. Wengler[7], N. Wermes[3], D. Wetterling[10,b1], G.W. Wilson[15,k], J.A. Wilson[1], G. Wolf[23], T.R. Wyatt[15], S. Yamashita[22], D. Zer-Zion[4], L. Zivkovic[20]

[1]School of Physics and Astronomy, University of Birmingham, Birmingham B15 2TT, UK
[2]Dipartimento di Fisica dell' Università di Bologna and INFN, I-40126 Bologna, Italy
[3]Physikalisches Institut, Universität Bonn, D-53115 Bonn, Germany
[4]Department of Physics, University of California, Riverside CA 92521, USA
[5]Cavendish Laboratory, Cambridge CB3 0HE, UK
[6]Ottawa-Carleton Institute for Physics, Department of Physics, Carleton University, Ottawa, Ontario K1S 5B6, Canada

[7]CERN, European Organisation for Nuclear Research, CH-1211 Geneva 23, Switzerland
[8]Enrico Fermi Institute and Department of Physics, University of Chicago, Chicago IL 60637, USA
[9]Fakultät für Physik, Albert-Ludwigs-Universität Freiburg, D-79104 Freiburg, Germany
[10]Physikalisches Institut, Universität Heidelberg, D-69120 Heidelberg, Germany
[11]Indiana University, Department of Physics, Bloomington IN 47405, USA
[12]Queen Mary and Westfield College, University of London, London E1 4NS, UK
[13]Technische Hochschule Aachen, III Physikalisches Institut, Sommerfeldstrasse 26-28, D-52056 Aachen, Germany
[14]University College London, London WC1E 6BT, UK
[15]School of Physics and Astronomy, Schuster Laboratory, The University of Manchester M13 9PL, UK
[16]Department of Physics, University of Maryland, College Park, MD 20742, USA
[17]Laboratoire de Physique Nucléaire, Université de Montréal, Montréal, Québec H3C 3J7, Canada
[18]University of Oregon, Department of Physics, Eugene OR 97403, USA
[19]Rutherford Appleton Laboratory, Chilton, Didcot, Oxfordshire OX11 0QX, UK
[20]Department of Physics, Technion-Israel Institute of Technology, Haifa 32000, Israel
[21]Department of Physics and Astronomy, Tel Aviv University, Tel Aviv 69978, Israel
[22]International Centre for Elementary Particle Physics and Department of Physics, University of Tokyo, Tokyo 113-0033, and Kobe University, Kobe 657-8501, Japan
[23]Particle Physics Department, Weizmann Institute of Science, Rehovot 76100, Israel
[24]Universität Hamburg/DESY, Institut für Experimentalphysik, Notkestrasse 85, D-22607 Hamburg, Germany
[25]University of Victoria, Department of Physics, P O Box 3055, Victoria BC V8W 3P6, Canada
[26]University of British Columbia, Department of Physics, Vancouver BC V6T 1Z1, Canada
[27]University of Alberta, Department of Physics, Edmonton AB T6G 2J1, Canada
[28]Research Institute for Particle and Nuclear Physics, H-1525 Budapest, P O Box 49, Hungary
[29]Institute of Nuclear Research, H-4001 Debrecen, P O Box 51, Hungary
[30]Ludwig-Maximilians-Universität München, Sektion Physik, Am Coulombwall 1, D-85748 Garching, Germany
[31]Max-Planck-Institute für Physik, Föhringer Ring 6, D-80805 München, Germany
[32]Yale University, Department of Physics, New Haven, CT 06520, USA

[a] and at TRIUMF, Vancouver, Canada V6T 2A3
[b] now at University of Alberta
[c] and Institute of Nuclear Research, Debrecen, Hungary
[d] now at Institute of Physics, Academy of Sciences of the Czech Republic 18221 Prague, Czech Republic
[e] and Department of Experimental Physics, University of Debrecen, Hungary
[f] and MPI München
[g] and Research Institute for Particle and Nuclear Physics, Budapest, Hungary
[h] now at University of Liverpool, Dept of Physics, Liverpool L69 3BX, U.K.
[i] now at Dept. Physics, University of Illinois at Urbana-Champaign, U.S.A.

[j] now at University of Texas at Arlington, Department of Physics, Arlington TX, 76019, U.S.A.
[k] now at University of Kansas, Dept of Physics and Astronomy, Lawrence, KS 66045, U.S.A.
[l] now at University of Toronto, Dept of Physics, Toronto, Canada
[m] current address Bergische Universität, Wuppertal, Germany
[n] now at University of Mining and Metallurgy, Cracow, Poland
[o] now at University of California, San Diego, U.S.A.
[p] now at The University of Melbourne, Victoria, Australia
[q] now at IPHE Université de Lausanne, CH-1015 Lausanne, Switzerland
[r] now at IEKP Universität Karlsruhe, Germany
[s] now at University of Antwerpen, Physics Department,B-2610 Antwerpen, Belgium; supported by Interuniversity Attraction Poles Programme – Belgian Science Policy
[t] now at Technische Universität, Dresden, Germany
[u] and High Energy Accelerator Research Organisation (KEK), Tsukuba, Ibaraki, Japan
[v] now at University of Pennsylvania, Philadelphia, Pennsylvania, USA
[w] now at TRIUMF, Vancouver, Canada
[x] now at Columbia University
[y] now at CERN
[z] now at DESY
[a1] now at Gjøvik University College, Pb. 191, 2802 Gjøvik, Norway
[b1] now at MWM GmbH Mannheim, Germany
[*] Deceased

1 Introduction

The formation of baryons within a jet of hadrons has proved difficult to model and is still not well understood. While the shape of momentum spectra can be derived from QCD with the modified leading logarithmic approximation together with parton-hadron duality [1], more complex observables like correlations have not been derived from first principles.

Several physical models like the thermodynamic [2], cluster fragmentation [3] or string fragmentation [4, 5] models, have been developed to describe baryon production. Of these, the most successful is string fragmentation, based on the creation of diquark-antidiquark pairs from the vacuum as illustrated in figure 1. In a production chain of particles along the string, a baryon and an antibaryon can be produced in immediate succession (figs. 1a,b) or else one or more intermediate mesons can be produced between them (figs. 1c-e). This production of intermediate mesons, referred to as the popcorn effect [6, 7], is included as an option in the Monte Carlo event generators JETSET and PYTHIA [8, 9] and can be steered with a free parameter.

Past experimental investigations of the popcorn effect made use of rapidity ordering of hadrons in the fragmentation chain. Intermediate mesons modify the rapidity difference between associated baryons and antibaryons. Rapidity correlations between $\Lambda\,\overline{\Lambda}$ pairs produced in Z^0 decays have been studied by several LEP collaborations and the conclusion was that best agreement between the experiments and the JETSET Monte Carlo model [8] was obtained

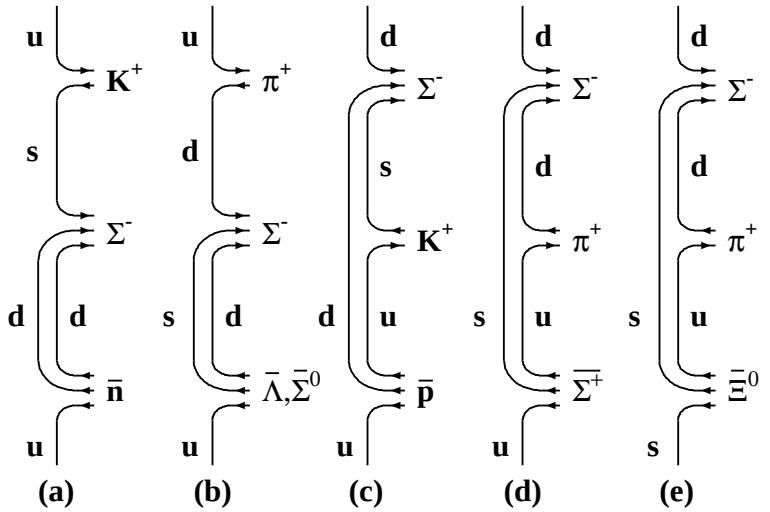

Figure 1: *Baryon production in the diquark model without (a,b) and with (c-e) the popcorn effect.*

with the popcorn effect included [10]-[12].

A contradictory result was reported by the DELPHI collaboration [13]. Their measurement is based on triple correlations between a proton, an antiproton and a charged pion close in rapidity. Because the popcorn effect enhances the pion density in the rapidity interval between the proton and antiproton, the minimum rapidity difference between a pion and a proton was compared for the particle orderings $p\pi\overline{p}$ and $\pi p\overline{p}$. The measurement indicated the absence of the popcorn effect. Insufficient modeling of the fragmentation dynamics could not, however, be excluded [13].

In this analysis, the popcorn mechanism is investigated in a different way, by tagging rare baryons and measuring the quantum numbers of correlated antibaryons. By not relying on rapidity differences, we obtain results that are more model-independent than previous studies. The data were collected with the OPAL experiment at the LEP e^+e^- collider at CERN. Especially suitable for our purposes is the Σ^- hyperon. If a Σ^- is produced, its baryon number and strangeness are compensated either by an antinucleon and a kaon, as illustrated in figure 1a, or by an associated antihyperon. The case of $\overline{\Lambda}$ or $\overline{\Sigma^0}$ production without the popcorn effect is shown in figure 1b.

The same graph, with the bottom-most u-quark replaced by a d- or s-quark, describes associated $\overline{\Sigma^-}$ and $\overline{\Xi^-}$ production. Associated production of a $\overline{\Sigma^+}$ and $\overline{\Xi^0}$ antihyperon with a Σ^- can only occur through the popcorn mechanism (figs. 1d,e). This makes $\Sigma^-\overline{\Sigma^+}$ and $\Sigma^-\overline{\Xi^0}$ correlations ideal tools to study the popcorn effect. Unfortunately, the production rate of Σ^- hyperons and the probabilities for simultaneous reconstruction of Σ^- and $\overline{\Sigma^+}$ or Σ^- and $\overline{\Xi^0}$ particles are too small to make such an analysis feasable, given the available data statistics. The equivalent analysis cannot be performed with tagged Λ hyperons because in this case $\overline{\Sigma^+}$ and $\overline{\Xi^0}$ antihyperons can be produced without the popcorn effect. Alternatively one can measure the fraction

$$F_{\overline{H}} = F_{\Sigma^-,\overline{\Sigma^-}} + F_{\Sigma^-,\overline{\Lambda}} + F_{\Sigma^-,\overline{\Xi^-}} \tag{1}$$

of Σ^- hyperons accompanied by a $\overline{\Sigma^-}$ ($F_{\Sigma^-,\overline{\Sigma^-}}$), a $\overline{\Lambda}$ ($F_{\Sigma^-,\overline{\Lambda}}$) or a $\overline{\Xi^-}$ ($F_{\Sigma^-,\overline{\Xi^-}}$). These correlations can occur in the popcorn model but are more likely in the diquark model (fig. 1b) and their rate is thus a sensitive measure of the baryon production mechanism.

The exact definition of the three correlations $F_{\Sigma^-,\overline{k}}$ in the sum (1) needs to account for the possibility that an event may contain more than one Σ^- hyperon, other additional hyperons, or more than one antihyperon. More generally, one can consider an arbitrary particle k and its antiparticle $\overline{k}$. If the number of Σ^- hyperons in an event is larger than 1, all combinations of Σ^- $\overline{k}$ and Σ^- k pairs are counted. Denoting the total rates of Σ^--antiparticle and Σ^--particle pairs by $R_{\Sigma^-,\overline{k}}$ and $R_{\Sigma^-,k}$, respectively, and the total Σ^- rate by R_{Σ^-}, the fraction $F_{\Sigma^-,\overline{k}}$ can be written as

$$F_{\Sigma^-,\overline{k}} = \frac{R_{\Sigma^-,\overline{k}} - R_{\Sigma^-,k}}{R_{\Sigma^-}} \ . \tag{2}$$

This definition implies that the $n_{\overline{k}}$ antiparticles $\overline{k}$ in an event enter $n_{\overline{k}}\, n_{\Sigma^-}$ times. The Σ^- Σ^- pairs are counted $n_{\Sigma^-}\,(n_{\Sigma^-}-1)$ times. In the data analysis, this multiple counting is not an issue because the number of reconstructed Σ^- hyperons per event is very small. Baryon number conservation ensures that $\sum_{\overline{k}} F_{\Sigma^-,\overline{k}} = 1$, if the sum extends over all antibaryons, including the antihyperons and antinucleons. It is the understanding throughout this paper that the charge conjugated channels are included. Thus, the rates $R_{\Sigma^-,k}$ contain all like-sign pairs Σ^- k and $\overline{\Sigma^-}$ $\overline{k}$, the rates $R_{\Sigma^-,\overline{k}}$ contain all unlike-sign pairs Σ^- $\overline{k}$ and $\overline{\Sigma^-}$ k, and $\overline{\Sigma^-}$ antihyperons are included in R_{Σ^-}.

It is evident from figure 1c that kaons created through the popcorn effect reduce $F_{\overline{H}}$. The PYTHIA Monte Carlo program without the popcorn effect, tuned to reproduce the observed baryon rates and momentum spectra, predicts $F_{\overline{H}} \approx 0.9$, as will be shown later. The other extreme is a model in which baryon number and strangeness are compensated statistically, i.e. from conservation laws alone. The ratio of weakly decaying hyperon to total baryon production in Z^0 decays is approximately 0.22 [14]. Because there must be at least one antibaryon in the rest of the event, if the Σ^- is detected, and the tagging biases the number of strange valence antiquarks, the lower bound will be a bit larger: $F_{\overline{H}} > 0.22$. A more rigorous calculation can be performed with the thermodynamic model for particle production. The advanced version of the model, based on the microcanonical ensemble, yields $F_{\overline{H}} = 0.23$ for an initial system without strangeness [15].

2 Event selection

2.1 Event topologies

In any experiment with a sufficiently large tracking device Σ^- hyperons can be identified by track kinks from $\Sigma^- \to \mathrm{n}\pi^-$ decays. At LEP energies, the efficiency is much less than 100%, because the decay vertex lies often outside the fiducial volume for its reconstruction. In principle, correlated decays $\overline{\Sigma^-} \to \overline{\mathrm{n}}\pi^+$ and $\overline{\Xi^-} \to \overline{\Lambda}\pi^+$ could be reconstructed using track kinks, too, but the efficiency for the exclusive reconstruction of $\Sigma^-\ \overline{\Sigma^-}$ or $\Sigma^-\ \overline{\Xi^-}$ pairs is small.

In this work, only the Σ^- hyperons were reconstructed exclusively. Two signatures for correlated antihyperons were used:

1. $\overline{\Lambda}$ hyperons were reconstructed by analyzing their so-called V^0 topology from the decay $\overline{\Lambda} \to \overline{\mathrm{p}}\pi^+$. The decay vertex and the flight direction of the $\overline{\Lambda}$ candidates allow the $\overline{\Lambda}$ impact parameters d_0 with respect to the beam line to be computed. Direct $\overline{\Lambda}$ production, including the contribution of decays from $\overline{\Sigma^0}$ hyperons, is characterized by low impact parameters d_0, while large impact parameters indicate a preceding weak decay and are a signature for $\overline{\Xi}$ decays.

2. Charged pions with significant impact parameters are a signature for weak decays of arbitrary antihyperons. An inclusive sample of tracks with large d_0 values, consistent with a pion interpretation, was selected. Throughout this paper, this data set is referred to as the sample of displaced tracks. This sample has a large background, and different antihyperon species contribute with different weights, because the number of decay pions per antihyperon is 1 for $\overline{\Sigma^-}$, 0.64 for $\overline{\Lambda}$ and 1.64 for chain decays of $\overline{\Xi^-}$.

The correlated $\Sigma^-\overline{\Lambda}$ candidate sample gives the numbers of true $\Sigma^-\ \overline{\Lambda}$ and $\Sigma^-\ \overline{\Xi^-}$ pairs. The fraction $F_{\overline{\Sigma^-}}$ can be extracted from the displaced track sample with a subtraction procedure, using this information as a constraint.

2.2 Experiment and data sets

All data taken by the OPAL experiment [16] in the Z^0 energy region during the years 1991 to 2000 were analyzed to measure the correlation. The OPAL experiment had nearly complete solid angle coverage and excellent hermeticity. The innermost part of the central tracking detector was a high-resolution silicon microvertex detector, which immediately surrounded the beam-pipe [17]. It was followed by a high-precision vertex drift chamber, a large-volume jet chamber [18], and z-chambers, all in a uniform 0.435 T axial magnetic field. In this work, the outer detector parts as well as the forward detector system were needed for triggering and identification of multihadronic events only. The criteria for multihadronic event selection have been described elsewhere [19].

The present analysis is entirely based on the central tracking system [16, 18]. For candidates to be accepted, all central wire chambers and the microvertex detector were required to be fully operational. The data sample for this analysis consists of 3.97 million events.

The identification of strange particles is based on earlier work [20, 21]. The innermost sense wires of the jet chamber had a distance of 25.5 cm from the beam spot, the wire-to-wire distance was 1 cm and there were 159 sensitive radial layers. The requirement of the pattern recognition program was the existence of at least 12 hits in the jet chamber. This makes it possible to identify Σ^- hyperons with decay lengths larger than 36 cm.

The z coordinate, along an axis parallel to the electron beam, was measured with a precision of 700 μm with the stereo wires of the vertex chamber and 100 to 350 μm with the z chambers. For tracks leaving the drift chamber at the side cones, the z coordinates of the exit points can be computed from the radius of the last wire with a hit. At the beam spot a constraint can be set using the bunch length of the beam. Inside the jet chamber, the z coordinates were measured with the charge division method with a resolution of 6 cm. This is one limiting factor for the kinematical reconstruction of Σ^- hyperons to be discussed later.

The quality of the impact parameter measurement is directly connected to the detector resolutions in the (r, φ) plane perpendicular to the beam axis. These resolutions were 5 μm to 10 μm for the microvertex detector [17], 55 μm for the vertex chamber and, on average, 135 μm for the jet chamber [16].

To study the detector response, the selection was applied also to Monte Carlo samples used before at OPAL. These were generated with the JETSET7.3 and JETSET 7.4 programs, followed by a full detector simulation [22]. The steering parameters for the generator are given in [23, 24]. The subset of parameters relevant for this analysis is discussed in section 4.2 and the numerical values are given in table 8 (appendix). In total, the Monte Carlo samples consisted of 4.65 million multihadronic Z^0 decays.

2.3 Σ^- Selection

The production cross section of Σ^- hyperons has previously been measured by OPAL [20]. Here the selection criteria to find track pairs forming a decay vertex were slightly changed relative to [20] to improve the sensitivity of the analysis to correlations. The applied cuts are summarized in table 1. They accommodate pattern recognition tolerances and define a fiducial jet chamber volume to guarantee minimal hit numbers for both tracks and to remove background from the end plates. The ratio l_1/p_1 in the last line of table 1 is proportional to the decay time in the rest frame of the decaying particle. High values are rejected to reduce the substantial background from kaon decays.

variable	condition
transverse momenta of the decaying and the daughter particle	$p_{T1} > 0.15$ GeV/c, $p_{T2} > 0.10$ GeV/c
total momentum of the decaying particle	$p_1 > 2$ GeV/c
impact parameter of the primary track	$d_0 < 5$ cm
endpoint radius of the primary track	$r_{E1} < 170$ cm
maximum gap between the primary and the secondary track in the (r, φ) plane	$d_{12} < 10$ cm
number of secondary tracks	1
particle charges	equal
arc distance between the intersection point and the end points of tracks 1,2 in (r, φ)	$\mu_1 > -7$ cm, $\mu_2 < +7$ cm
radius of the intersection point	$r_{Vtx} > 35$ cm
distance of the intersection point from the end plate in z direction	$\Delta z_{Vtx} > 40$ cm
χ^2 for agreement of the two tracks in the (r, φ) plane, using (3×3) error matrix	$\chi^2 > 2000$
ratio of the track length to the momentum of the decaying particle	$l_1/p_1 < 15$ cm/(GeV/c)

Table 1: *Selection of track pairs forming a decay vertex (for a more detailed description of the variables, see [20]).*

Monte Carlo studies show that the following processes have to be considered as sources for Σ^- candidates, others being negligible [20]:

1. $\Sigma^- \to \mathrm{n}\pi^-$;
2. $\overline{\Sigma^+} \to \overline{\mathrm{n}}\pi^-$;
3. $\Xi^- \to \Lambda\pi^-$;
4. $\mathrm{K}^- \to \pi^-$+neutrals; $\mathrm{K}^- \to \mu^-$+neutrals or $\mathrm{K}^- \to e^-$+neutrals;
5. secondary reactions in the detector material and fake background. The last sample consists mainly of scattered particles.

To determine the relative contributions of these processes to the observed data sample, an unfolding procedure very similar to that used in [20] was used. The invariant mass m_{Σ^-} and the decay angle θ^* of the pion candidate in the rest frame of the hypothetical Σ^- particle were computed, assuming that the unseen neutral particle is a neutron. The angle θ^* is defined with respect to the flight direction of the Σ^- candidate at the decay vertex.

Figure 2 shows scatter plots of these variables for the data and three Monte Carlo sources of events with kinked tracks, namely events with Σ^-, Ξ^- or K^- in the final state. The background 5, not shown in figure 2, is a smooth function of both observables and is largest in the backward direction $\cos\theta^* = -1$.

Five two-dimensional regions, denoted by $a, ...e$, were introduced in the $(m_{\Sigma^-}, \cos\theta^*)$ plane to enrich dedicated kink sources (see figure 2). The bin number of a Σ^- candidate was used as an observable in the unfolding procedure to be described in section 3.

In total, 16790 candidates were found in the two-dimensional plane in the mass range from threshold to 1.5 GeV. In the Monte Carlo sample 18754 kinks were identified.

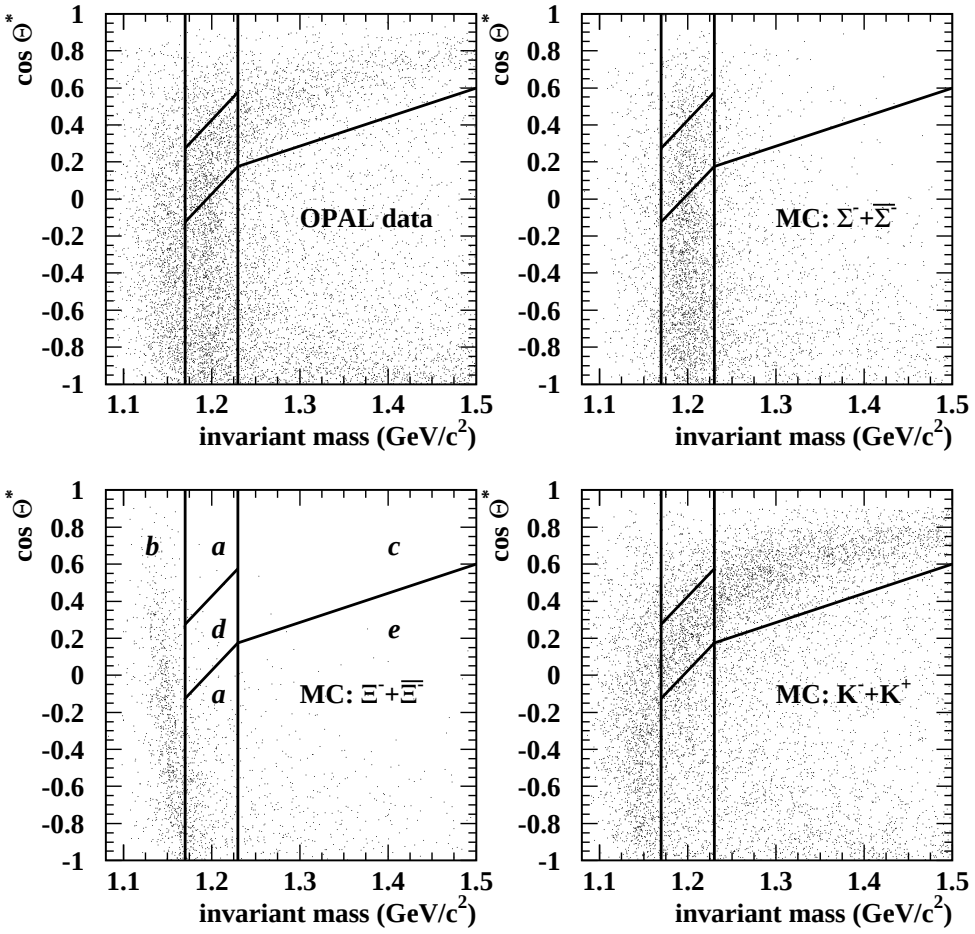

Figure 2: *Definition of two-dimensional bins to disentangle Σ^- hyperons from background. The reconstructed mass is plotted versus the pion emission angle in the hypothetical center-of-mass system. Top left: data. Other plots: Monte Carlo simulations for three particle classes as indicated. The labeling of the two-dimensional bins is shown in the bottom left plot. The preferential bins for the kink sources are: a+d for Σ^- and $\overline{\Sigma^+}$, b for Ξ^-, b,c and d for K^- and e for background.*

2.4 Selection of pions from weak decays

Two pre-cuts were applied to select tracks with a good reconstruction quality: the transverse momentum with respect to the beam had to be larger than 0.15 GeV/c and the track angle at the beam spot relative to the beam direction was restricted to the region $|\cos\theta| \leq 0.80$.

To remove charged particles from charm or bottom decays, the impact parameter $d_{0,\pi}$ with respect to the primary vertex was required to be larger than 0.2 cm. This cut is the essential condition to define the sample of displaced tracks. A lower value would be sufficient but does not improve the accuracy of the correlation analysis.

Pions were enriched using the specific energy loss measurement of the central drift chamber [26]. A weight $w_{dE/dx}(\pi)$ was defined as the probability that the energy loss dE/dx of a pion deviates from the median value $< dE/dx > (\pi)$ by more than the measured difference from the median value. The applied condition was $w_{dE/dx}(\pi) > 0.02$ and the number of hits contributing to this measurement had to be at least 20.

Finally, the angle between the momenta of the pion candidate and the Σ^- candidate at the primary vertex was required to be less than 90 degrees. This hemisphere cut is motivated by the fact that it rarely happens that baryon number and strangeness are compensated by an antihyperon in the opposite event hemisphere. The cut reduces the combinatorial background by a factor 2.

In total, 9965 correlated like-sign $\Sigma^-\pi^-$ and 11951 unlike-sign Σ^- π^+ pair candidates were selected with these cuts. The corresponding results for the Monte Carlo sample are 10769 and 13818, respectively. If the total number of Monte Carlo track kinks is scaled to the observation, the number of like-sign pairs in the data is well reproduced by the Monte Carlo, the difference being $(+3.4 \pm 1.4)\%$. The observed unlike-sign minus like-sign difference, however, deviates from the prediction by $(-28 \pm 7)\%$. This deficit, already visible at raw data level, indicates that the Monte Carlo sample contains too many correlated antihyperons and is the basis for the final result of this paper.

2.5 Λ Selection

The selection cuts to find Λ decays in the central drift chamber have been described in [21]. The preselection cuts were relaxed from those of [21]. In this analysis all candidates with reconstructed masses between the pπ threshold and 1.20 GeV/c^2 were accepted. This larger mass window was needed to study the non-Λ background.

Two criteria were added. If the reconstructed Λ flight path points back to the (r, φ) position of the hypothetical Σ decay kink within 2 degrees, it was assumed that the kink originated from a $\Xi^- \rightarrow \Lambda\pi^-$ decay and the Λ candidate was dropped. The cut removed approximately 3/4 of the like sign Ξ^- Λ ($\overline{\Xi^-}$ $\overline{\Lambda}$)-pairs and reduced the self-correlation of Ξ^- particles with their own decay Λ's accordingly.

Secondly, the hemisphere cut applied to the decay pions was also applied to the Λ's. The

angle between the flight directions of Σ and $\overline{\Lambda}$ at the primary vertex was required to be less than 90 degrees.

For the correlation analysis, the mass window was reduced to a ± 10 MeV wide interval around the true Λ mass. Totals of 276 $\Sigma^-\Lambda$ ($\overline{\Sigma^-}\,\overline{\Lambda}$) and 604 $\Sigma^-\,\overline{\Lambda}$ ($\overline{\Sigma^-}\,\Lambda$) pair candidates passed all selection cuts. In the Monte Carlo sample 284 like-sign and 721 unlike-sign pairs were found. The observed unlike-sign minus like-sign difference is smaller than the Monte Carlo prediction by $(16 \pm 11)\%$, if normalized to the number of observed kinks.

3 Correlation analysis

3.1 Unfolding of kink sources

From the Monte Carlo sample one gets, for every kink source i and every two-dimensional $(m_{\Sigma^-}, \cos\theta^*)$ bin j, the number of accepted events $K_i^{(MC)}(j)$. The populations of the bins $j = a,\ldots e$ in figure 2 are sensitive to the invariant mass and θ^* resolutions, which in turn depend on the z resolution of the central drift chamber. The z coordinate, however, is not well modeled in the Monte Carlo simulation. Because the track end points in the jet chamber are well known by other measurements, this mismodeling at the decay vertex gives the dominant contribution to the systematic error of the Σ^- rate [20]. To correct the Monte Carlo program for it, the z components of all Σ momenta were modified according to $p_{z\cdot new} = p_{z,rec} + c \cdot (p_{z,rec} - p_{z,true})$, where $p_{z,true}$ is the true momentum from the MC generator and $p_{z,rec}$ the reconstructed momentum. The constant c is one common factor to be determined in the analysis.

The total number of kinks $K(j)$ expected in bin j is given by

$$K(j) = \sum_i \xi_i \frac{N_{data}}{N_{MC}} \cdot K_i^{(MC)}(j) \ , \tag{3}$$

where N_{data} and N_{MC} are the total number of multihadronic data and Monte Carlo events, respectively. Incorrect Monte Carlo rates are corrected for by the five scaling factors ξ_i. If they are known, the true production rates per multihadronic event, R_i, can be computed for all sources i, for example

$$R_{\Sigma^-} = \xi_{\Sigma^-} \cdot R_{\Sigma^-}^{(MC)} \quad \text{with} \quad R_{\Sigma^-}^{(MC)} = \sum_j K_{\Sigma^-}^{(MC)}(j) \ . \tag{4}$$

Contrary to [20] the factors ξ_i were treated as momentum independent, because the analysis of [20] had shown that the modeling of the spectral shape was satisfactory. The contribution from $\overline{\Sigma^+}$ hyperons to $K(j)$ is less than 20% of that of the Σ^- particles [20]. The ratio of the genuine production rates, approximately 1 due to isospin symmetry, was fixed to the Monte Carlo prediction, so that $\xi_{\overline{\Sigma^+}} = \xi_{\Sigma^-}$. Four scaling factors ξ_i were thus left for adjustment. They were computed with a χ^2-fit of the measured kink rates to equation (3) for a given value of c.

It was then checked whether the Monte Carlo simulation reproduces the reconstructed mass and $\cos\theta^*$ distributions. Differing from our previous analysis [20], the proportionality factor c was chosen to get the lowest χ^2-sum for both distributions. The best overall agreement was found for $c = 1.35$ with a one-sigma interval ranging from 1.32 to 1.45. The final fit result is shown in figs. 3 and 4. The agreement is excellent. The error of c is not included in the statistical errors of the ξ_i. It is treated separately as a contribution to the systematic error.

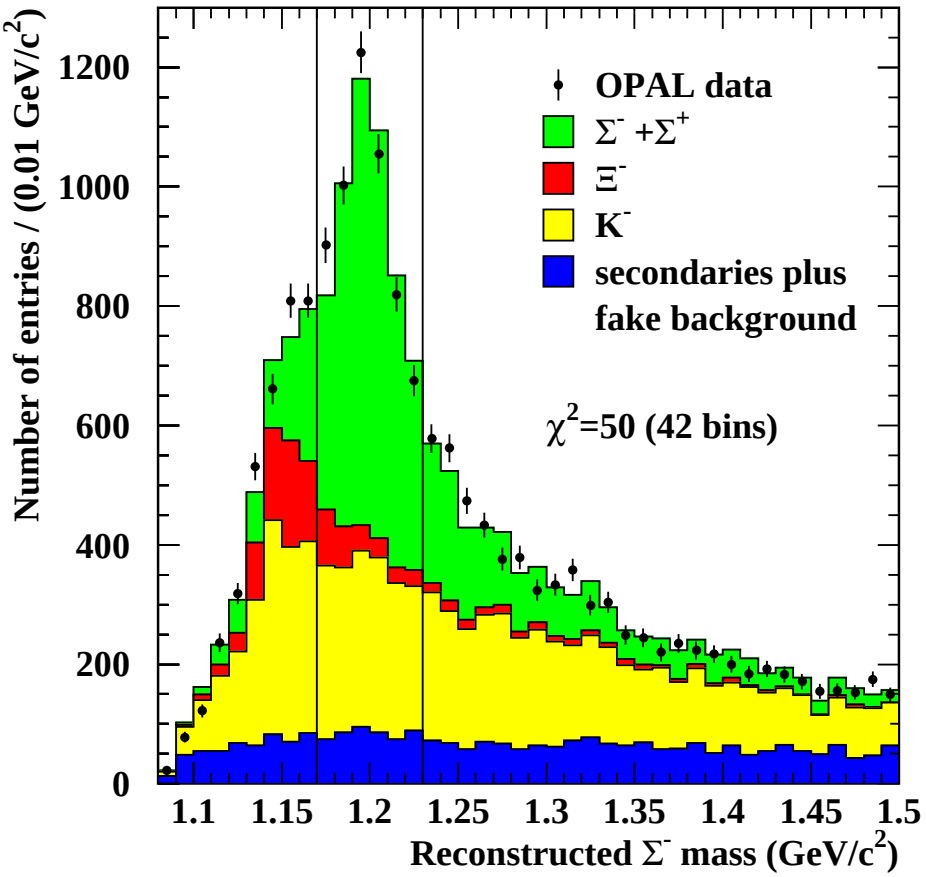

Figure 3: *Measured Σ^- mass spectrum. Points: data. Histograms: results of the fit, ordered according to the sources for track kinks. The plotted errors are the statistical errors of the data.*

The $\Sigma^- + \overline{\Sigma^-}$ production rate was found to be $R_{\Sigma^-} = 0.073 \pm 0.004$. According to [20] a systematic error of ± 0.009 has to be added. Within the total error, this result is consistent with our published value $R_{\Sigma^-} = 0.083 \pm 0.011$. The difference is mainly due to the modified treatment of the z-resolution.

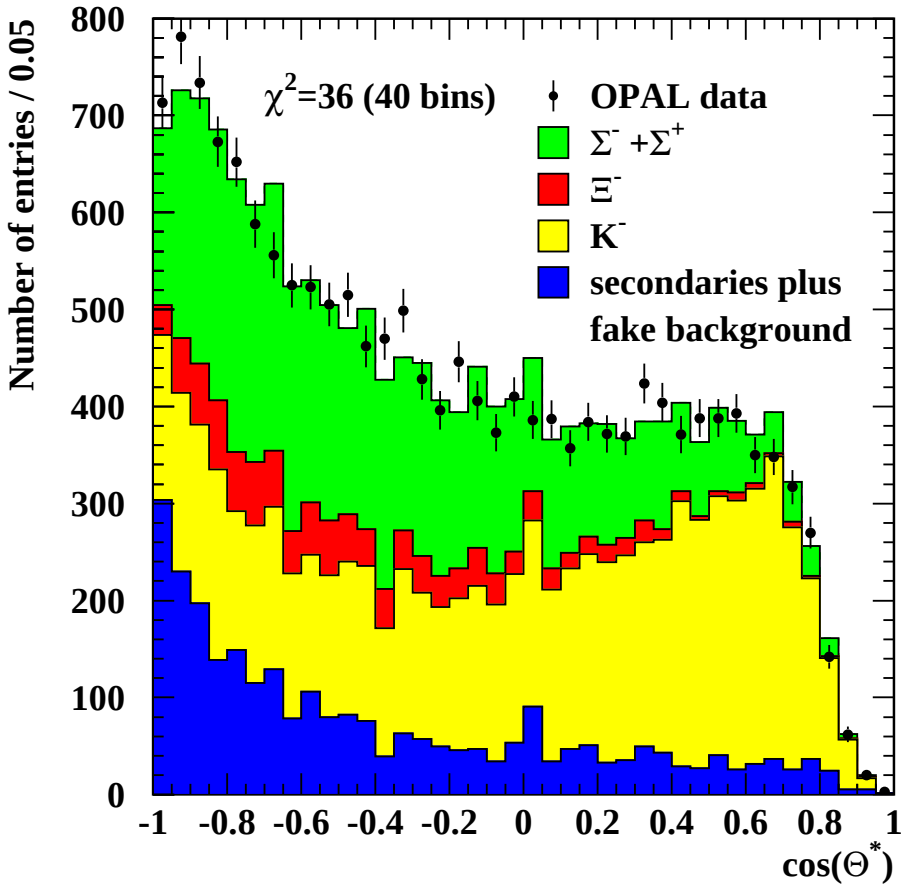

Figure 4: *Cosine of the center-of-mass pion emission angle. Points: data. Histograms: results of the fit, ordered according to the sources for track kinks. The plotted errors are the statistical errors of the data.*

3.2 Correlated particle sources

The correlated rates of kink-V^0 or kink-displaced-track pairs were measured as a function of the bin number j and the impact parameter d_0 of the correlated particle relative to the beam line. The variable d_0 contains information on the lifetime of the parent particle of the correlated particle in case of a preceding weak decay, and is needed to disentangle correlated $\overline{\Lambda}$'s from $\overline{\Xi}$'s decaying into $\overline{\Lambda}$'s.

In the Monte Carlo simulation, nine sources have to be considered for the displaced tracks and correlated V^0's:

1. $\overline{\Sigma^-} \rightarrow \overline{\mathrm{n}}\pi^+$;
2. $\overline{\Sigma^+} \rightarrow \overline{\mathrm{n}}\pi^-$ or $\overline{\mathrm{p}}\pi^0$;
3. $\overline{\Xi^-} \rightarrow \overline{\Lambda}\pi^+ \rightarrow \overline{\mathrm{p}}\pi^+\pi^+$;
4. $\overline{\Xi^0} \rightarrow \overline{\Lambda}\pi^0 \rightarrow \overline{\mathrm{p}}\pi^+\pi^0$;
5. $\overline{\Lambda} \rightarrow \overline{\mathrm{p}}\pi^+$, including $\overline{\Lambda}$ antihyperons from $\overline{\Sigma^0}$ decays, but without the contributions from $\overline{\Xi}$ decays;
6. charged particles from K^+ decays;
7. charged particles or V^0 configurations from K^0 decays;
8. non-K^0 background of the V^0 topology;
9. displaced tracks from secondary interactions, mainly scattering.

All sources, except for the eighth one, contribute to the sample of displaced tracks. For V^0-like events only the sources 3,4,5,7 and 8 are relevant. The sample of displaced tracks is enriched in pions but contains also a small fraction of protons and leptons. These contaminations are included in the Monte Carlo rates and are classified according to the above scheme.

The combination of five kink sources with nine correlated particle sources leads to a total number of 45 classes of particle pairs. In addition, one has to distinguish between like-sign and unlike-sign pairs. Equation (3) can be generalized to the like-sign pair rate $D^{like}(j, d_0)$ and the difference of the unlike-sign pair rate $D^{unlike}(j, d_0)$ and $D^{like}(j, d_0)$,

$$D^{like}(j, d_0) = \sum_{i,k} \eta_{i,k}^{(l)} \cdot \frac{N_{data}}{N_{MC}} \cdot D_{i,k}^{(MC,like)}(j, d_0) \ ; \tag{5}$$

$$D^{unlike}(j, d_0) - D^{like}(j, d_0) = \sum_{i,k} \eta_{i,k}^{(a)} \cdot \frac{N_{data}}{N_{MC}} \cdot (D_{i,k}^{(MC,unlike)}(j, d_0) - D_{i,k}^{(MC,like)}(j, d_0)) \ . \tag{6}$$

The indices at the Monte Carlo rates $D_{i,k}^{(MC,like)}$ and $D_{i,k}^{(MC,unlike)}$ specify the kink source i and the correlated particle source k, respectively. The parameters $\eta_{i,k}^{(l)}$ and $\eta_{i,k}^{(a)}$ are 90 scaling

kink source	correlated particle					
	$\overline{\Sigma^-}$	$\overline{\Sigma^+}$	$\overline{\Xi^-}$	$\overline{\Xi^0}$	$\overline{\Lambda}$	K^+
Σ^-	0.33	0.014	0.15	0.01	0.28	0.04
Σ^+	0.01	0.32	0.01	0.14	0.28	0.024
Ξ^-	0.34	0.026	0.15	0.029	0.36	0.45
K^-	< 0.01	< 0.01	< 0.01	< 0.01	0.03	0.50

Table 2: *Fractions $F_{i,k}^{(MC)}$ as predicted by the PYTHIA 6.1 generator with the parameters from ref [24].*

factors. In principle, they have to be extracted with a combined fit of the j and d_0 dependent distributions of kink-track pairs and kink-V^0 pairs to equations (5) and (6).

The Monte Carlo generator predicts the generic correlations $F_{i,\overline{k}}^{(MC)}$, defined with equation (2), generalized to arbitrary sources i and k. Table 2 gives the results for hyperon-antiparticle correlations at generator level for the most recent parameter set used by the OPAL experiment [24].

If the scaling factors $\eta_{i,k}^{(a)}$ are known, the experimental results for the correlations can be computed

$$F_{i,\overline{k}} = \frac{\eta_{i,k}^{(a)}}{\xi_i} \cdot F_{i,\overline{k}}^{(MC)} \ . \tag{7}$$

Here, the scaling factors ξ_i from the kink fit (section 3.1) enter.

The factors $\eta_{i,k}^{(l)}$ are only needed to parameterize the statistical errors for the fit using equation (6). With very few exceptions, they are close to one and no physical result is extracted from them.

3.3 Evaluation of the correlation matrix

In spite of the large number of scaling factors $\eta_{i,k}^{(a)}$, a reliable fit of the data can be obtained. This can be seen from the integrals of the differences $(D_{i,k}^{(MC,unlike)}(j,d_0) - D_{i,k}^{(MC,like)}(j,d_0))$ over the variables $m_{\Sigma^-}, \cos\theta^*$ and d_0, listed in tables 3 and 4. The entries in the tables are normalized to the total differences, using $\eta_{i,k}^{(a)} = 1$, and thus show the relative importance of the terms. Many correlations are very small. If not given in the tables explicitly, the contribution of a source is less than 2%. The entries in table 3 for displaced tracks account for 96% of the total rate difference. The contributions to the V^0 in table 4 add up to 104%, the excess being compensated by a small amount of $\Sigma^+\overline{\Lambda}$ correlations with the opposite sign.

The scaling factors for the four largest correlations in tables 3 and 4, $\eta^{(a)}_{\Sigma^-,\overline{\Sigma^-}}$, $\eta^{(a)}_{\Sigma^-,\overline{\Lambda}}$, $\eta^{(a)}_{\Sigma^-,\overline{\Xi^-}}$ and $\eta^{(a)}_{\Xi^-,\overline{\Lambda}}$, are determined with the fit. Three of them are needed to compute $F_{\overline{H}}$.

kink source	displaced track source				
	$\overline{\Sigma^-}$	$\overline{\Xi^-}$	$\overline{\Lambda}$	K^+	background
Σ^-	$(27 \pm 1)\%$	$(16 \pm 1)\%$	$(10 \pm 1)\%$		$(17 \pm 4)\%$
Ξ^-	$(12 \pm 1)\%$	$(6 \pm 1)\%$	$(5 \pm 1)\%$		
K^-				$(3 \pm 1)\%$	
kink background					

Table 3: *Largest contributions to the correlations between kinks and displaced tracks.*

kink source	V^0 source		
	$\overline{\Xi^-}$	$\overline{\Lambda}$	V^0 background
Σ^-	$(20 \pm 2)\%$	$(43 \pm 3)\%$	$(14 \pm 3.5)\%$
Ξ^-	$(6 \pm 1.5)\%$	$(21 \pm 2)\%$	

Table 4: *Largest contributions to the correlations between kinks and V^0 candidates.*

The data statistics do not allow to fit more than four parameters. The remaining η's were thus fixed by symmetry considerations, isospin invariance or Monte Carlo studies. Systematic errors were assigned to them, if necessary. In the following, a few examples are described, preferentially the correlations in tables 3,4.

For symmetry reasons, one has

$$\eta^{(a)}_{\Xi^-,\overline{\Sigma^-}} = \eta^{(a)}_{\Sigma^-,\overline{\Xi^-}} \ . \tag{8}$$

There is no model independent prediction for $F_{\Xi^-,\overline{\Xi^-}}$. This parameter was set to the original Monte Carlo result. It follows then from equation (7) that

$$\eta^{(a)}_{\Xi^-,\overline{\Xi^-}} = \xi_{\Xi^-} \ . \tag{9}$$

It has been checked for various acceptable Monte Carlo generator tunings, described in the next section, that this procedure is valid within 20%.

Non-negligible parts of the correlation are introduced by the correlated particle backgrounds 8 and 9; they are given as sums over the kink sources in tables 3 and 4. The origin of this effect is charge conservation in the events. Since the displaced-track-background consists mainly of scattered particles, it reflects the original particle charges. The kink selection introduces a charge bias for the rest of the event, which is visible in the ensemble of remaining charged particles on a statistical basis. This is true not only for scattered particles, but also for asymmetric fake V^0 candidates. Kinks and correlated particles are assigned to each other by chance. The condition $\eta^{(a)}_{i,track} = \eta^{(a)}_{i,V^0} = \xi_i$ was introduced, assuming a correct modeling of the background sources 8 and 9. This is justified because the equivalent relation for the like-sign background rates was confirmed with a fit to the data with the parameterizations $\eta^{(l)}_{i,track} = \xi_i \zeta_{track}$ and $\eta^{(l)}_{i,V^0} = \xi_i \zeta_{V^0}$, the results being $\zeta_{track} = 1.01 \pm 0.04$ and $\zeta_{V^0} = 1.03 \pm 0.07$, respectively.

The remaining entry in table 3 is the charged kaon-kaon correlation. Its contribution is small because kaon decay inside the jet chamber is unlikely due to the long kaon life time. Since

the charged and neutral kaon production rates are almost equal and the hyperon rates are much smaller than the kaon rates, the fraction F_{K^-,K^+} is close to 0.5 so that $\eta^{(a)}_{K^-,K^+} = \xi_{K^-}$.

No model independent prediction exists for $F_{K^-,\overline{\Lambda}}$, which was determined with the Monte Carlo event sample. A correlation potentially dangerous for the fit is the $\Sigma^-\mathrm{K}^+$ correlation. The corresponding asymmetry in table 2 is small, but actually it is the difference of much larger components. Strangeness conservation requires

$$F_{\Sigma^-,\overline{\Sigma^-}} + F_{\Sigma^-,\overline{\Sigma^+}} + 2 \cdot F_{\Sigma^-,\overline{\Xi^-}} + 2 \cdot F_{\Sigma^-,\overline{\Xi^0}} + F_{\Sigma^-,\overline{\Lambda}} + 2 \cdot F_{\Sigma^-,K^+} \approx 1 \ . \tag{10}$$

The parameters $F_{\Sigma^-,\overline{\Xi^-}}$ and $F_{\Sigma^-,\overline{\Xi^0}}$ appear with the weight 2 because the Ξ-particles carry two units of strangeness. The contribution from $\overline{\Omega^-}$ hyperons is negligible. The factor 2 in front of F_{Σ^-,K^+} accounts for the $\overline{\mathrm{K}^0}$ contribution, which cannot be measured. Monte Carlo simulations with different model parameters showed that relation (10) is fulfilled within 3%. Together with the condition for baryon number conservation,

$$F_{\Sigma^-,\overline{\Sigma^-}} + F_{\Sigma^-,\overline{\Sigma^+}} + F_{\Sigma^-,\overline{\Xi^-}} + F_{\Sigma^-,\overline{\Xi^0}} + F_{\Sigma^-,\overline{\Lambda}} + F_{\Sigma^-,\overline{p}} + F_{\Sigma^-,\overline{n}} \approx 1, \tag{11}$$

equation (10) gives the relation

$$F_{\Sigma^-,K^+} \approx \frac{1}{2} \cdot (F_{\Sigma^-,\overline{p}} + F_{\Sigma^-,\overline{n}} - F_{\Sigma^-,\overline{\Xi^-}} - F_{\Sigma^-,\overline{\Xi^0}}) \ , \tag{12}$$

which shows the presence of large compensating terms. In the analysis, F_{Σ^-,K^+} was therefore computed with the sum rule (10), taking the small correlations $F_{\Sigma^-,\overline{\Sigma^+}}$ and $F_{\Sigma^-,\overline{\Xi^0}}$ from the Monte Carlo generator. Similarly, F_{Ξ^-,K^+} can be constrained by the equivalent equation for the Ξ^-,

$$F_{\Xi^-,\overline{\Sigma^-}} + F_{\Xi^-,\overline{\Sigma^+}} + 2 \cdot F_{\Xi^-,\overline{\Xi^-}} + 2 \cdot F_{\Xi^-,\overline{\Xi^0}} + F_{\Xi^-,\overline{\Lambda}} + 2 \cdot F_{\Xi^-,K^+} \approx 2 \ . \tag{13}$$

The correlations of the Σ^+ hyperons are related to those of the Σ^- hyperon by the isospin symmetry, for instance $F_{\Sigma^+,\overline{\Lambda}} = F_{\Sigma^-,\overline{\Lambda}}$.

The above relations allow either to replace $\eta^{(a)}_{i,k}$ by the four factors to be fitted, or to fix it and its contribution to the right hand side of equation (6). A simultaneous binned χ^2 fit, using equation (6), was performed for the d_0 distributions of the correlated-track and Λ candidates in the five $(m_{\Sigma^-}, \cos\theta^*)$-regions. In the Λ case, the reconstructed mass was restricted to the narrow interval given in section 2.5. In parallel, a fit of the like sign pairs to equation (5) was performed to determine $\zeta_{track} = \eta^{(l)}_{i,track}/\xi_i$ and three normalization factors for the hyperon-$\overline{\Lambda}$, K^--hyperon and (Σ^- or Ξ^-) – ($\overline{\Sigma^-}$ or $\overline{\Xi^-}$) correlations. The statistical errors of the pair rates, needed to compute χ^2, were computed with the equations (5) and (6); they depend on the result of the fit. The fit was therefore done iteratively, setting the unknown η-factors to unity for the first iteration. The statistical errors had d_0 dependent fluctuations due to the limited Monte Carlo statistics. These were reduced with a one-dimensional smoothing algorithm described in [25]. The asymmetry fit resulted in a χ^2 value of 144 for 146 degrees of freedom. The coefficients obtained are correlated, the largest correlation coefficient being $\approx$-0.7 between $\eta^{(a)}_{\Sigma^-,\overline{\Sigma^-}}$ and $\eta^{(a)}_{\Sigma^-,\overline{\Xi^-}}$.

3.4 Experimental results and systematic errors

The adjusted d_0 distributions are shown in figs. 5 and 6. The histograms give the contributions of the correlated particle sources; all kink sources and two-dimensional bins $j = a,\ldots e$ are combined. The errors of the data points are statistical and the corresponding errors of the Monte Carlo histograms are not shown. Fig. 7 gives the rate differences between the unlike-sign and like-sign kink-V^0 pairs as a function of the reconstructed Λ mass. Both distributions are very well described.

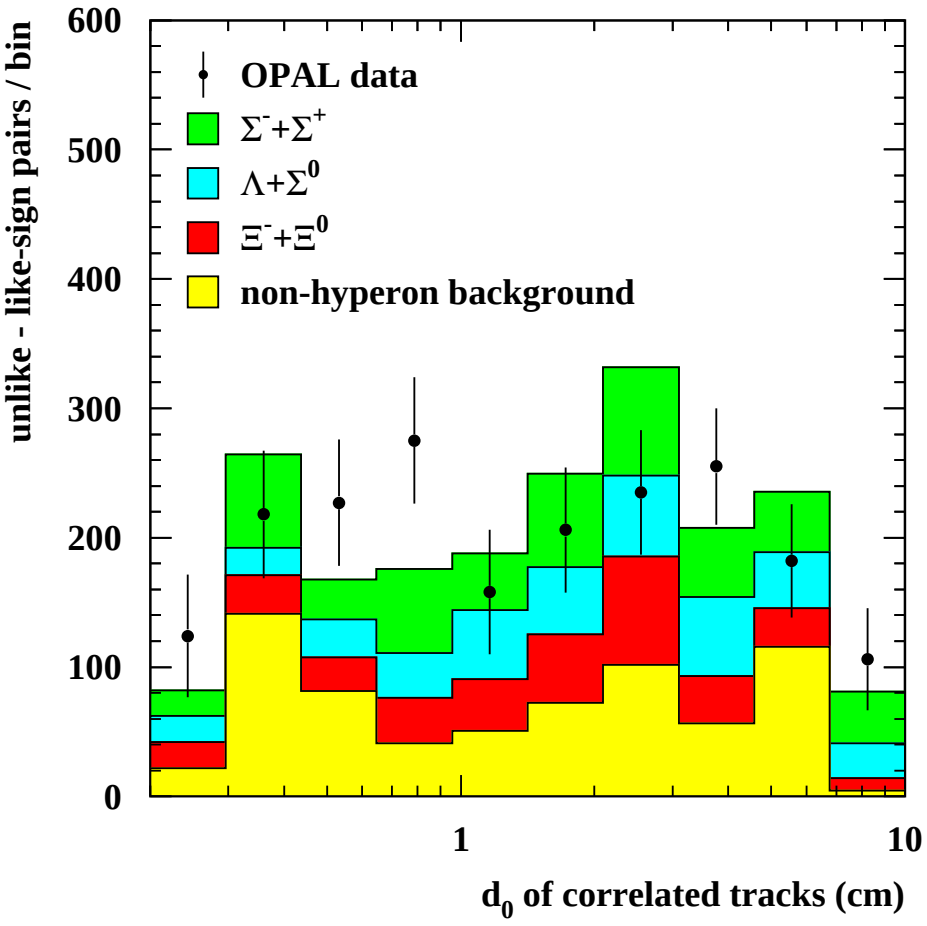

Figure 5: *Impact parameters of the displaced tracks, correlated to Σ^- candidates. The difference between unlike-sign and like-sign combinations is shown. Points: data. Histograms: results of the fit, ordered according to the sources for displaced tracks. The plotted errors are the statistical errors of the data.*

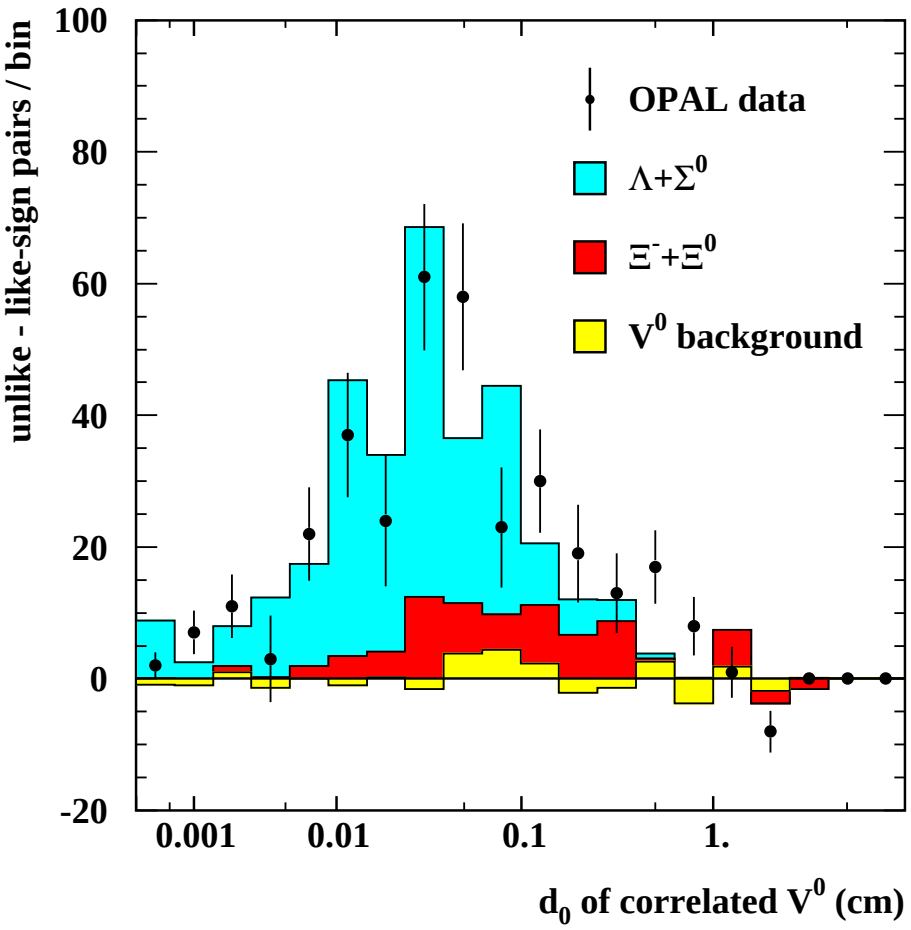

Figure 6: *Impact parameters of the* $\overline{\Lambda}$ *candidates, correlated to* Σ^- *candidates. The difference between unlike-sign and like-sign combinations is shown. Points: data. Histograms: results of the fit, ordered according to the* V^0 *sources. The plotted errors are the statistical errors of the data.*

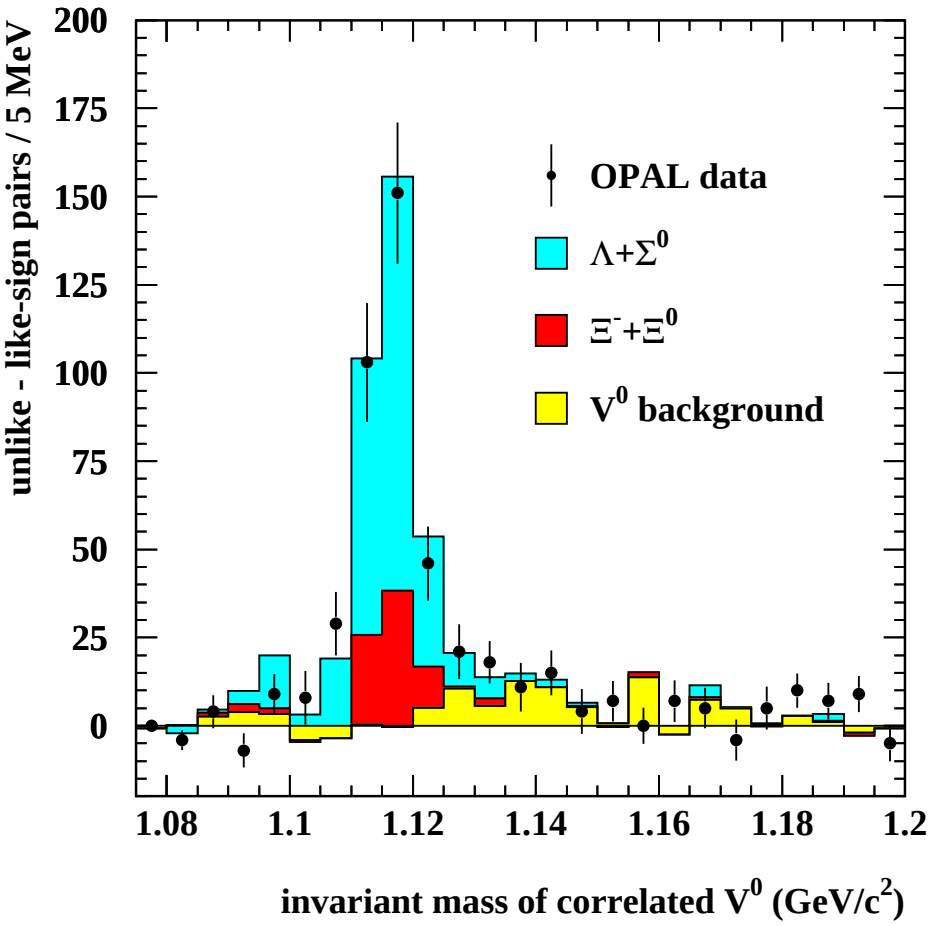

Figure 7: *Reconstructed masses of the $\overline{\Lambda}$ candidates, correlated to Σ^- candidates. The difference between unlike-sign and like-sign combinations is shown. Points: data. Histograms: results of the fit, ordered according to the V^0 sources. The plotted errors are the statistical errors of the data.*

	correlation			
	$F_{\Sigma^-,\overline{\Sigma^-}}$	$F_{\Sigma^-,\overline{\Xi^-}}$	$F_{\Sigma^-,\overline{\Lambda}}$	$F_{\overline{H}}$
fit result	0.162 ± 0.100	0.054 ± 0.047	0.234 ± 0.057	0.449 ± 0.091
systematic error				
mismodeling of correlated particle momenta	$+0.009$ ± 0.005	$+0.003$ ± 0.002	$+0.014$ ± 0.007	$+0.026$ ± 0.013
z-resolution at kink vertex	± 0.037	± 0.023	± 0.045	± 0.024
dE/dx calibration	± 0.010	± 0.005	± 0.004	± 0.008
hemisphere cut	± 0.005	± 0.002	± 0.007	± 0.013
number of hits per track	± 0.007	± 0.004	± 0.002	± 0.006
$\cos\theta$ distribution of tracks	± 0.012	± 0.001	± 0.001	± 0.012
Λ detection efficiency	± 0.006	± 0.004	± 0.004	± 0.002
charge asymmetry of detection efficiencies	± 0.002	± 0.001	± 0.001	± 0.002
uncertainty of popcorn channels	± 0.008	± 0.005	± 0.004	± 0.007
uncertainty of $\Xi^-\overline{\Xi^-}$ correlation	± 0.003	± 0.001	± 0.001	± 0.003
uncertainty of $\mathrm{K}^-\overline{\Lambda}$ correlation	± 0.001	± 0.001	± 0.003	± 0.002
final result	0.17 ± 0.11	0.057 ± 0.056	0.25 ± 0.08	0.48 ± 0.10

Table 5: *Experimental results and systematic errors.*

The fit results are listed in the first row of table 5. The errors are statistical and include the data and Monte Carlo contributions. Internally, the fit gets the Λ part of the correlation essentially from the correlated Λ sample, which sets also bounds on $F_{\Sigma^-,\overline{\Xi^-}}$. The $\Sigma^-\overline{\Sigma^-}$ correlation is computed from the displaced-track sample as a difference. Neither $F_{\Sigma^-,\overline{\Sigma^-}}$ nor $F_{\Sigma^-,\overline{\Xi^-}}$ differ from zero in a statistical way, in contrast to the overall sum $F_{\overline{H}}$. The smaller error of the sum is due to the strong anti-correlation between $F_{\Sigma^-\overline{\Sigma^-}}$ and $F_{\Sigma^-,\overline{\Xi^-}}$. The final results, including the systematic errors, are given in the last row of table 5.

The systematic errors, listed in table 5, will be discussed in the following.

Mismodeling of correlated particle momenta. The momentum spectra of the correlated pion and Λ candidates are not well reproduced by the Monte Carlo program. The simulated momenta have to be scaled downwards by as much as 20%. The effect exists both for the like sign and the unlike-sign track and V^0 candidates. As a consequence, the measured fractions $F_{i,\overline{k}}$ are systematically too small. To find a correction, the detection efficiencies for the correlated particles were extracted from the Monte Carlo sample and the shifted momentum spectrum was folded with the efficiency function. This leads to an upwards correction of the measured correlations. A global correction of $(6 \pm 3)\%$ was applied. This correction, together with its error, is much larger than the uncertainties

due to miscalibrations of the particle momenta or the impact parameters. Therefore, no additional errors were assigned to the momentum and d_0 selection cuts.

z-resolution at kink vertex. In the ratio of a correlated rate to the single Σ^- rate the overall detection efficiency for Σ^- hyperons cancels. However, an uncertainty of the number of observed Σ^- hyperons arises from the unfolding procedure. The dominating error source is the mismodeling of the z-resolution. The correction factor c, introduced above, was conservatively varied between 1.25 and 1.5. For the individual correlations $F_{\Sigma^-,\overline{k}}$ the obtained shifts were found to be non-parabolic functions of c. The maximal shifts of the results $F_{\Sigma^-,\overline{k}}$ and $F_{\overline{H}}$ were taken as uncertainties.

dE/dx calibration. Any antiproton impurity in the displaced track sample reduces the asymmetry from direct or indirect $\overline{\Lambda}$ decays. For a pure pion sample and a perfect calibration, the frequency distribution of the weight $w_{dE/dx}(\pi)$, defined in section 2.4, should not depend on $w_{dE/dx}(\pi)$. A superimposed peak at $w_{dE/dx}(\pi) = 0$ is expected due to non-pions. The shape of this peak does not perfectly agree with the Monte Carlo prediction. A systematic error was assigned to the corresponding mismodeling of the antiproton rejection efficiency.

Hemisphere cut. In principle, the results are corrected automatically for the hemisphere cut. No significant correlations were observed in the dropped hemisphere. A systematic error would appear, if the fragmentation model were incorrect. A 3% error was assigned to all correlations, based on the error of the number of tracks in the omitted hemisphere.

Other systematic errors The number of hits per track is well modeled and introduces an error of 1% for the number of displaced tracks. Also the acceptance cut for the θ angle plays a minor role only. From the difference between the angular distributions of data and Monte Carlo events an efficiency error of 3% was estimated. Systematic errors due to the cuts for Λ selection were already discussed in [21]. An uncertainty of $\pm 3.3\%$ was taken from that paper as fully correlated error for the Λ event sample. Differences $\Delta\epsilon_i$ between the detection efficiencies for particles and antiparticles would lead to a spurious asymmetry, if both the kinks i and the correlated particles k are affected. The effect is proportional to $\Delta\epsilon_{\Sigma^-} \cdot \Delta\epsilon_k$. The efficiency differences were extracted from the observed particle and antiparticle rates and the upper limits for the spurious asymmetries in table 5 were obtained. Furthermore, there are uncertainties due to the model dependence of the correlations which had to be subtracted. One half of the Monte Carlo baryon antibaryon pairs are accompanied by a popcorn meson. The $\eta^{(a)}$-factors for the popcorn specific correlations $\Sigma^-\overline{\Sigma^+}$, $\Sigma^-\overline{\Xi^0}$ and $\Xi^-\overline{\Sigma^+}$ were varied between 0 and 2 and the fit repeated. The $\mathrm{K}^-\overline{\Lambda}$ correlation was varied by 50% and an uncertainty of 20% was assigned to the $\Xi^-\overline{\Xi^-}$ correlation, fixing the small residual contribution from Ξ^- self correlations. As already mentioned, the definition of $F_{\overline{H}}$ introduces a small amount of double counting, both in the data and in the Monte Carlo simulation. This problem was studied with a toy Monte Carlo program and the only effects found were negligible corrections to the statistical errors of the fit.

The correlated kink-track and kink-V^0 pairs should be concentrated in the Σ^- enriched bins a and d in the $(m_{\Sigma^-}, \cos\theta^*)$ plane shown in figure 2. As a cross check, a simpler analysis was performed, where the analysis was restricted to region a. All background asymmetries

and also the $\Xi^-\overline{\Lambda}$ correlation were subtracted as predicted by the Monte Carlo program. The final result including reevaluated systematic errors, $F_{\overline{H}} = 0.472 \pm 0.155$, is fully consistent with the main result and demonstrates the absence of anomalies in the $(m_{\Sigma^-}, \cos\theta^*)$ plane.

4 Comparison with fragmentation models

Before comparing the result for $F_{\overline{H}}$ to the predictions of models, we adjusted the models, incorporated into the PYTHIA Monte Carlo event generator, to describe a set of observables in Z^0 decays. The optimization began with the PYTHIA steering parameters given in [24]. These were slightly modified to reproduce the newest experimental information on the baryonic sector, including data on $\Lambda\overline{\Lambda}$ correlations. The tuned Monte Carlo was then used to predict $F_{\overline{H}}$. We also used the models to study $p\pi\overline{p}$ correlations more extensively than previously, as described below.

4.1 Observables

The input observables for the tuning fall into four categories:

1. Eight baryon multiplicities in multihadronic Z^0 decay: p, Δ^{++}, Λ, $\Sigma^+ + \Sigma^-$, Σ^0, Ξ^-, $\Sigma^{*+} + \Sigma^{*-}$, and Ω^-. The production rates were taken from the compilation of the particle data group [14].

2. Proton and Λ momentum spectra. Baryon spectra have approximately Gaussian shapes if parameterized in terms of the variable $\xi = \ln(1/x_p)$ [1]. We use the mean values and variances of the proton and Λ spectra as the observables. Deviations from the normal distribution are known, the true maxima being somewhat higher than the result of the fit [27, 31]. However, the Gaussian fit is an easy way to compare different experiments. The tabulated data [27]–[31] were fitted to Gaussian functions in the interval $1.2 < \xi < 4.2$. The situation for the protons is not satisfactory, the fitted maxima of the ξ distributions varying from 2.79 [28] to 3.08 [31]. The values $\xi_{peak} = 2.80 \pm 0.07$ and $\sigma = 1.11 \pm 0.06$ were obtained with a combined fit using all LEP and SLD data. The errors were not taken from the fit but conservatively estimated from the systematic differences between the ξ spectra of the experiments. It should be noted that both ξ_{peak} and σ depend on the fit range due to deviations of the ξ-distribution from the Gaussian shape. The agreement between experiments is better for Λ production, leading to values $\xi_{peak} = 2.62 \pm 0.04$ and $\sigma = 1.21 \pm 0.04$.

3. $\Lambda\overline{\Lambda}$ correlations. The correlation was parameterized by two observables, the first one being the rate excess of $\Lambda\ \overline{\Lambda}$ pairs over $\Lambda\ \Lambda\ +\ \overline{\Lambda}\ \overline{\Lambda}$ pairs per event, $N^{corr}_{\Lambda\overline{\Lambda}}$. The other observable is the mean rapidity difference $\overline{\Delta y}_{\Lambda\overline{\Lambda}}$ between the Λ and $\overline{\Lambda}$ after subtraction of like-sign pairs. The number of correlated $\Lambda\ \overline{\Lambda}$ pairs per event was taken from [12]. The mean $\Lambda\overline{\Lambda}$ rapidity difference $\overline{\Delta y}$ was computed from the data of [12], as the truncated mean for $\Delta y < 3.0$. This cut was introduced to suppress the contribution of Λ's from the opposite event hemisphere.

4. Nine meson production rates per multihadronic Z^0 decay: $\pi^+ + \pi^-$, π^0, $K^+ + K^-$, K^0_S, $\rho^+ + \rho^-$, ρ^0, φ, $K^{*+}(892) + K^{*-}(892)$ and $K^{*0}(892)$. These rates, taken from [14], were included in the tuning to protect the meson generation against parameter modifications steering the baryonic sector.

4.2 Model Parameters

The popcorn mechanism is incorporated in PYTHIA in two ways [9]. The first **simple version** was originally introduced in JETSET. Baryon production is controlled by the following parameters:

1. the suppression of diquark-antidiquark production relative to quark-antiquark production, $\mathbf{P}(qq)/\mathbf{P}(q)$ = PARJ(1);
2. the suppression of $s\overline{s}$ production relative to $u\overline{u}$ production, $\mathbf{P}(s)/\mathbf{P}(u)$ = PARJ(2); a tuning of this parameter was necessary, because the strange meson rates had to be readjusted;
3. a double ratio involving diquarks containing s quarks, $(\mathbf{P}(us)/\mathbf{P}(ud))/(\mathbf{P}(s)/\mathbf{P}(u))$ = PARJ(3);
4. the suppression factor for spin 1 diquarks, $(1/3)\mathbf{P}(ud_1)/\mathbf{P}(ud_0)$ = PARJ(4);
5. the popcorn parameter, which determines the relative occurrences of the baryon-meson-antibaryon and baryon-antibaryon configurations, PARJ(5);
6. an extra suppression for having an $s\ \overline{s}$ pair in a baryon-meson-antibaryon configuration, PARJ(6);
7. an extra suppression for having a strange meson in a baryon-meson-antibaryon configuration, PARJ(7);
8. a parameter which enters the exponent of the Lund symmetric fragmentation function for diquarks, PARJ(45); this parameter has an impact on the rapidity difference in baryon-antibaryon correlations.

In the **advanced popcorn** scheme, a universal equation for tunneling from the vacuum is applied to the generation of new partons and an arbitrary number of mesons can be created between a baryon and an antibaryon. The tunneling probability is proportional to $\exp(-\beta_q \cdot M_\perp)$, where β_q is a flavor dependent model parameter and $M_\perp$ the transverse mass of the created object. Only the first two and the last parameter of the above list are used in this scheme. There are three new parameters, two of them related to the tunneling formula:

9. the tunneling coefficient for u-quarks, β_u = PARJ(8);
10. $\delta\beta = \beta_s - \beta_u$ = PARJ(9)
11. an extra suppression factor for spin 3/2 baryons = PARJ(18).

popcorn parameter PARJ(5)		0.	0.5	1.	5.	
observable	data	MC1	MC2	MC3	MC4	MC5 advanced popcorn
χ^2	-	56	59	59	63	99
$N^{corr}_{\Lambda\overline{\Lambda}}$	0.0612 ± 0.0034	0.066	0.060	0.066	0.058	0.081
$\overline{\Delta y}_{\Lambda\overline{\Lambda}}$	0.71 ± 0.04	0.66	0.69	0.67	0.75	0.57
$F_{\Sigma^-,\overline{\Sigma^-}}$ (this work)	0.17 ± 0.11	0.39	0.34	0.30	0.19	0.20
$F_{\Sigma^-,\overline{\Xi^-}}$ (this work)	0.057 ± 0.056	0.18	0.16	0.15	0.09	0.08
$F_{\Sigma^-,\overline{\Lambda}}$ (this work)	0.25 ± 0.08	0.30	0.28	0.28	0.27	0.28
$F_{\overline{H}}$ (this work)	0.48 ± 0.10	0.87	0.79	0.73	0.55	0.56

Table 6: *Comparison with fragmentation models. Fit quality χ^2, $\Lambda\overline{\Lambda}$ correlations and the Σ^- antihyperon correlations as defined in the text. The errors of the simulation are smaller than the last digit shown.*

4.3 Simulation Results

For a given PYTHIA parameter set, the measured observables from section 4.1 were compared with the simulation results and a χ^2 was computed. It cannot be expected from a fragmentation model that all its predictions are correct to better than a few percent. To reduce the contributions of very accurately measured observables, the errors to compute χ^2 were thus taken to be at least 2.5%. Low χ^2 values were searched for with the method described in the appendix, for fixed values of the popcorn parameter. Many tunes of the generator have almost the same quality. Some PYTHIA parameter sets and the predicted baryon production rates are given in the appendix. Table 6 shows the χ^2's, the $\Lambda\overline{\Lambda}$ correlations and the Σ^--antihyperon correlations, as a function of the popcorn parameter, where the simple popcorn model is denoted MC1 to MC4.

The variable χ^2 is an indicator for the quality of the baryon modeling. For the simple popcorn model, the lowest χ^2 value found was 56 for the 23 observables. This means that the Monte Carlo generator describes, on average, the observables roughly within 2 times the experimental errors or 5%, whichever is larger.

The most important result of the simulation is that the overall quality of the description of the observables does not depend strongly on the popcorn parameter in the simple popcorn model. The $\Lambda\overline{\Lambda}$ correlation parameters are always reproduced within two standard deviations, whether the popcorn effect is switched on or off. The Monte Carlo parameter space examined here is larger than that in earlier studies. In view of the overall uncertainty it is not possible to reach a definite conclusion about the the popcorn effect by using $\Lambda\overline{\Lambda}$ correlations.

As shown in the bottom line of table 6, the measured fraction $F_{\overline{H}}$ is consistent both with the predictions of the original popcorn model with a large popcorn parameter (MC4) and the optimized advanced popcorn model (MC5), but is smaller than the Monte Carlo prediction

for zero popcorn effect. To investigate the stability of this last simulation result, the relevant parameters of the PYTHIA generator, especially the diquark fragmentation function, were randomly varied as described in the appendix. In these studies, $F_{\overline{H}}$ values less than 0.86 were not obtained. The experimental result deviates from this lower limit by 3.8 standard deviations.

The advanced popcorn model has fewer parameters available for tuning and provides a significantly worse description of data as seen from the larger χ^2 value. The larger χ^2 for this model arises to a large extent from two well known facts. The absolute number of $\Lambda\ \overline{\Lambda}$ pairs is too large and the distribution of the $\Lambda\ \overline{\Lambda}$ rapidity differences is too narrow in comparison to the observation [12]. On the other hand, the average $\Lambda\overline{\Lambda}$ rapidity difference in the simple popcorn model with a very large popcorn parameter is too large, so that a combination of the two models might possibly describe the $\Lambda\overline{\Lambda}$ correlation well.

To complete the comparison of correlations with results from Monte Carlo generators, the DELPHI $\mathrm{p}\pi\overline{\mathrm{p}}$ [13] correlation was also investigated. This was done for rapidity ordered $\mathrm{p}\pi\overline{\mathrm{p}}$ and $\pi\mathrm{p}\overline{\mathrm{p}}$ or $\mathrm{p}\overline{\mathrm{p}}\pi$ particle configurations inside event hemispheres. The selection cuts and the definition of the minimum rapidity gap Δy_{min} between a selected pion and the next proton were taken from [13]. The discriminating variable of [13] is the ratio of intensities

$$R(\Delta y_{min}) = \frac{N(\mathrm{p}\pi\overline{\mathrm{p}})}{N(\mathrm{p}\pi\overline{\mathrm{p}}) + N(\pi\mathrm{p}\overline{\mathrm{p}} + \mathrm{p}\overline{\mathrm{p}}\pi)} \tag{14}$$

at the rapidity difference Δy_{min}. A strong dependence on the popcorn effect had been seen by [13] at large values of Δy_{min}. For three bins in the range $0.625 \leq \Delta y_{min} \leq 1$, the observed distribution agreed with a subsample of Monte Carlo events without the popcorn mechanism and disagreed with a disjunct subsample, containing popcorn mesons, by more than five standard deviations, averaged over the three bins.

These results could be reproduced with the simulations described here: The R distributions obtained with the parameter set MC1, but without detector corrections, agreed with DELPHI's observation within 1.9 standard deviations, while there was disagreement between the data and Monte Carlo study MC2 by 5.2 standard deviations, averaged over the same three Δy_{min} bins. Variations of the fragmentation model had not been studied in [13]. An increase of the fragmentation parameter PARJ(45) to unity, fixing the other parameters of the simulation MC2, reduces the difference between the data and the model prediction to 2.4 standard deviations. Furthermore, it was found that the advanced popcorn model with the parameter set MC5 results in almost the same function $R(\Delta y_{min})$ as the model MC1 without the popcorn effect.

The modification of the parameter PAR(45) in the simulation MC2 increased the χ^2 value in table 6 from 59 to 70 due to a shift of $\overline{\Delta y}_{\Lambda\overline{\Lambda}}$ to a value below the observation, without degrading the description of the other observables of section 4.1. In summary, these results indicate a high sensitivity of the rapidity correlations to the fragmentation dynamics.

popcorn parameter PARJ(5)		0.	0.5	1.	5.	
observable	data	MC1	MC2	MC3	MC4	MC5 advanced popcorn
protons	1.046 ± 0.026	1.03	1.03	1.02	1.09	1.01
Δ^{++}	0.087 ± 0.033	0.098	0.118	0.122	0.122	0.127
Λ	0.388 ± 0.009	0.369	0.362	0.366	0.388	0.388
$\Sigma^+ + \Sigma^-$	0.181 ± 0.018	0.129	0.131	0.129	0.133	0.141
Σ^0	0.076 ± 0.010	0.069	0.070	0.069	0.070	0.073
Ξ^-	0.0258 ± 0.0009	0.029	0.029	0.028	0.029	0.024
$\Sigma^*(1385)^{+,-}$	0.046 ± 0.004	0.043	0.048	0.052	0.051	0.054
Ω^-	0.0016 ± 0.0003	0.0005	0.0004	0.0004	0.0004	0.0004

Table 7: *Baryon rates per multihadronic event. The errors of the simulation are smaller than the last digit shown.*

5 Conclusions

Our investigations indicate that the fragmentation models have not yet reached a state where they can quantitatively describe the $\Lambda\overline{\Lambda}$ correlations, the $p\overline{p}\pi$ correlations and the Σ^- antihyperon correlation $F_{\overline{H}}$ simultaneously. Neither the $\Lambda\overline{\Lambda}$ nor the $p\overline{p}\pi$ correlations can provide a clear conclusion about the popcorn effect because they can both be described to an acceptable level by models either with and without the popcorn mechanism. The PYTHIA generator without the popcorn effect can reproduce both rapidity correlations simultaneously within two standard deviations. Both correlations are also in acceptable agreement with model predictions including the popcorn effect. However, we were unable to find a variant of the popcorn model that could simultaneously describe both types of correlations.

In this work, the mechanism of baryon formation was studied by counting Σ^- hyperons and correlated antihyperons from hadronic Z^0decays. The result $F_{\overline{H}} = 0.48 \pm 0.10$, based on data taken by the OPAL experiment at LEP, favors a large popcorn parameter in the simple popcorn model and is also consistent with the advanced popcorn model. The fragmentation dynamics play no role here because the rapidity is not used in the analysis. Correlated particle momenta play an indirect role only, because they influence the detection efficiencies, but the final result contains a correction and a systematic error for mismodeling.

Trivial correlations between hyperons and antihyperons based on baryon number and strangeness conservation, as predicted by the thermodynamic model, always exist. Due to the limited data statistics and the insensitivity to the dynamics, our result gives only a weak indication for non-trivial quark correlations between baryon-antibaryon pairs. Statistical models, only constrained by conservation laws, differ at most by 2.6 standard deviations.

The result for $F_{\overline{H}}$ deviates from the lower limit of simulations without the popcorn effect by 3.8 standard deviations and thus demonstrates the existence of the popcorn effect. Any fragmentation model with very strong valence quark correlations between baryons and

model parameter	standard OPAL tune	MC1	MC2	MC3	MC4	MC5 advanced popcorn
PARJ(5)	0.5	0.	0.5	1.	5.	-
PARJ(1)	0.085	0.092	0.100	0.101	0.117	0.226
PARJ(2)	0.31	0.33	0.33	0.34	0.34	0.31
PARJ(3)	0.45	0.32	0.41	0.40	0.48	-
PARJ(4)	0.025	0.055	0.029	0.021	0.007	-
PARJ(6)	0.5	-	0.33	0.56	0.35	-
PARJ(7)	0.5	-	0.21	0.20	0.28	-
PARJ(8)	-	-	-	-	-	1.00
PARJ(9)	-	-	-	-	-	2.07
PARJ(18)	-	-	-	-	-	0.18
PARJ(45)	0.5	0.16	0.22	0.52	0.33	0.27

Table 8: *Parameter sets used for the simulations in tables 6 and 7.*

MC parameter	PARJ(1)	PARJ(2)	PARJ(3)	PARJ(4)	PARJ(45)
mean value	0.091	0.31	0.35	0.045	0.50
interval	± 0.008	± 0.04	± 0.08	± 0.012	± 0.50

Table 9: *Parameter ranges used for random generation of Monte Carlo parameter sets without the popcorn effect.*

antibaryons is disfavored.

Appendix: Tuning of the Monte Carlo generator

The tuning started with the PYTHIA parameters of [24], listed as "standard OPAL tune" in table 8. In a first step, the parameters, except the popcorn parameter, were varied individually and minimum values of χ^2 were searched for. This process was iterated. Search ranges for all parameters were defined either by requiring a maximum increase in χ^2 of 20 or, in the case of smaller changes, by allowing a parameter shift of $\pm 100\%$. Finally, all parameters were varied randomly within these ranges to search for χ^2 values lower than that of the solution already found. Between 200 and 300 random parameter sets were generated at fixed PARJ(5) for the final search and 10^5 events were generated per parameter set. The results for the selected parameters sets MC1 to MC5 are based on 10^6 events. The contributions of the four classes of observables to χ^2 at the minimum value 56 are about 40 from the baryon rates, 10 from the meson rates and 6 from the remaining six observables.

The measured and simulated baryon rates per Z^0 decay are given in table 7, while the corresponding PYTHIA parameters are listed in table 8. The Ω^- baryon was included in the optimization to avoid its almost complete suppression. The results for the parameter sets MC3 and MC5 are similar to those in our previous publication [12], where the case without the

popcorn effect was not investigated. The reproduction of the meson sector does not change much during the tuning and is therefore omitted from table 7.

Finally, table 9 gives the parameter space for the study of the parameter dependence of $F_{\overline{H}}$. All cases with $\chi^2 < 110$ were kept, allowing average discrepancies between the data and the model as large as those obtained with the modified popcorn model.

Acknowledgments

We are grateful to F.Becattini for applying the thermodynamic model to the Σ^- antihyperon correlations and we thank J.Lamsa and K.Hamacher from the DELPHI collaboration for discussions about the proton-antiproton-pion correlations. We particularly wish to thank the SL Division for the efficient operation of the LEP accelerator at all energies and for their close cooperation with our experimental group. In addition to the support staff at our own institutions we are pleased to acknowledge the
Department of Energy, USA,
National Science Foundation, USA,
Particle Physics and Astronomy Research Council, UK,
Natural Sciences and Engineering Research Council, Canada,
Israel Science Foundation, administered by the Israel Academy of Science and Humanities,
Benoziyo Center for High Energy Physics,
Japanese Ministry of Education, Culture, Sports, Science and Technology (MEXT) and a grant under the MEXT International Science Research Program,
Japanese Society for the Promotion of Science (JSPS),
German Israeli Bi-national Science Foundation (GIF),
Bundesministerium für Bildung und Forschung, Germany,
National Research Council of Canada,
Hungarian Foundation for Scientific Research, OTKA T-038240, and T-042864,
The NWO/NATO Fund for Scientific Research, the Netherlands.

References

[1] Y. L. Dokshitzer, V. A. Khoze, S. I. Troyan, Z. Phys. **C55** (1992) 107;
Int. J. Mod. Phys. **A7** (1992) 1875.

[2] F. Becattini, Z. Phys. **C69** (1996) 485;
J. Phys. **G23** (1997) 1933.

[3] G. Marchesini *et al.*, Comp. Phys. Comm. **67** (1992) 465.

[4] B. Andersson, G. Gustafson, G. Ingelman and T. Sjöstrand, Phys. Rep. **97** (1983) 31.

[5] B. Andersson, G. Gustafson and T. Sjöstrand, Nucl. Phys. **B197** (1982) 45.

[6] B. Andersson, G. Gustafson and T. Sjöstrand, Phys. Scripta **32** (1985) 574.

[7] P. Eden and G. Gustafson, Z. Phys. **C75** (1997) 41.

[8] T. Sjöstrand, Comp. Phys. Comm. **92** (1994) 74.

[9] T. Sjöstrand *et al.*, Comp. Phys. Comm. **135** (2001) 238.

[10] ALEPH Collaboration, D. Busculic *et al.*, Z. Phys. **C64** (1994) 361.

[11] DELPHI Collaboration, P. Abreu *et al.*, Phys. Lett. **B416** (1998) 247;
DELPHI Collaboration, P. Abreu *et al.*, Phys. Lett. **B318** (1993) 249.

[12] OPAL Collaboration, G. Abbiendi *et al.*, Eur. Phys. J. **C13** (2000) 185;
OPAL Collaboration, P. Acton *et al.*, Phys. Lett. **B305** (1993) 415.

[13] DELPHI Collaboration, P. Abreu *et al.*, Phys. Lett. **B490** (2000) 61.

[14] Review of Particle Properties, C. Amsler *et al.*(Particle Data Group), Phys. Lett. **B669** (2008) 1.

[15] F. Becattini and G. Passaleva, Eur. Phys. J. **23** (2002) 551;
F. Becattini, private communication.

[16] OPAL Collaboration, K. Ahmet *et al.*, Nucl. Instr. Meth. **A305** (1991) 275.

[17] P. Allport *et al.*, Nucl. Instr. Meth. **A324** (1993) 34;
P. Allport *et al.*, Nucl. Instr. Meth. **A346** (1994) 476.

[18] O. Biebel *et al.*, Nucl. Instr. Meth. **323** (1992) 169.

[19] OPAL Collaboration, G. Alexander *et al.*, Z. Phys. **C52** (1991) 175.

[20] OPAL collaboration, G. Alexander *et al.*, Z. Phys. **C73** (1997) 587.

[21] OPAL collaboration, G. Alexander *et al.*, Z. Phys. **C73** (1997) 569;
OPAL Collaboration, P. D. Acton *et al.*, Phys. Lett. **B291** (1992) 503.

[22] J. Allison *et al.*, Nucl. Instr. Meth. **A317** (1992) 47.

[23] OPAL Collaboration, P. D. Acton *et al.*, Z. Phys. **C58** (1993) 387.

[24] OPAL Collaboration, G. Alexander *et al.*, Z. Phys. **C69** (1996) 543.

[25] P. Bock, JHEP **08** (2006) 56.

[26] M. Hauschild *et al.*, Nucl. Instr. Meth. **A314** (1992) 74.

[27] DELPHI Collaboration, P. Abreu *et al.*, Eur. Phys. J. **C5** (1998) 585.

[28] ALEPH Collaboration, R. Barate *et al.*, Eur. Phys. J. **C5** (1998) 205;
ALEPH Collaboration, Phys. Rep. **204** (1998) 1.

[29] OPAL Collaboration, R. Akers etal, Z. Phys. **C63** (1994) 181.

[30] ALEPH Collaboration, R. Barate *et al.*, Eur. Phys. J. **C16** (2000) 613;
L3 Collaboration, M. Acciari *et al.*, Phys. Lett. **B407** (1997) 389;
DELPHI Collaboration, P. Abreu *et al.*, Phys. Lett. **318** (1993) 249.

[31] SLD Collaboration, K. Abe *et al.*, Phys. Rev. **D69** (2004) 072003.